AH- Thesis   070
Bla
Ana
ms

ANALYTICAL REMOVAL OF ATMOSPHERIC ABSORPTIONS

FROM REMOTELY SENSED NEAR-INFRARED DATA OF

GEOLOGICAL TARGETS

A THESIS SUBMITTED TO THE GRADUATE DIVISION OF THE
UNIVERSITY OF HAWAII IN PARTIAL FULFILLMENT
OF THE REQUIREMENTS FOR THE DEGREE OF

MASTER OF SCIENCE

IN GEOLOGY AND GEOPHYSICS

DECEMBER 1983

By

Pamela Lea Blake

Thesis Committee:

Robert B. Singer, Chairman
Thomas B. McCord
Michael J. Gaffey

We certify that we have read this thesis and that in our opinion it is satisfactory in scope and quality as a thesis for the degree of Master of Science in Geology and Geophysics.

THESIS COMMITTEE

_____
Chairman

_____

_____

ACKNOWLEDGEMENTS

Thank-you, Dr. Roger Clark, for SPECPR — you don't know how many times I've appreciated these routines.

This thesis would not have been even remotely (no pun intended ...) possible without the knowledge and efforts of the engineering and computer staff, particularly Karl Hinck, Mark Rognstad, Jeff Bosel and Jeff Hoover. And I especially thank Jeff Hoover and Tim Jackowski for their conscientiously applied skill in bringing SPECPR up so quickly on the VAX during those last desperate hours.

I sincerely thank Sam Ostrowski, Zeny Cocson, and all the administrative staff for maintaining the organization of this organization.

I extend a special thanks to Dr. Peter Mouginis-Mark and to Dr. B. Ray Hawke for their late-night support and companionship, for cheering up those otherwise lonely computer nights.

And thank-you (appearing in alphabetical order) Aaron, Dr. Bob Brown, Chuck, Ed, Jeff, Lisa, Dr. Lucy McFadden (gone, but not forgotten!), Marcia, Paul, Sue, and Trude — Good Luck, Gang!

Finally, I give my eternal thanks and love to Dr. David Isaak and Jean Brady for their unfailing generous love. Without these two people, nothing would be possible.

ABSTRACT

INTRODUCTION

A method has been developed to remove the effects of absorption by the atmosphere from remotely-sensed near-infrared reflectance spectra of geological objects on the earth's surface. This method is unique in that it does not make reference to an external reflectance standard, but instead utilizes the remotely-obtained spectra themselves to provide the information to calibrate out the atmospheric contribution to these same spectra. Removal of the effects of the atmosphere on remotely-obtained data is required because atmospheric absorptions (principally water-vapor) overlap, and are generally of greater magnitude than, absorptions resulting from geological materials. The technique presented here was developed using raw, uncalibrated remotely-sensed near-infrared (0.6μm to 2.6μm) reflectance spectra obtained in the field.

DATA SET

The data set used to develop and test this technique consisted of high-resolution ($\Delta\lambda/\lambda$ = 1.5%) near-infrared spectra of several rock samples measured both remotely in the field and in the laboratory using a state-of-the-art circularly variable filter (CVF) indium antimonide (InSb) astronomical spectrophotometer. The samples consisted of two basalts, a carbonate, and a white reflectance standard. These samples were measured in the field at a distance of approximately 0.5 km.

TECHNIQUE

The remotely-obtained spectra were used in conjunction with a set of synthetic atmospheric transmission spectra generated using the LOWTRAN model and code developed by McClatchey et al. (1972) and Kneizys et al. (1980). The raw field data were used to provide the basis for assessing the atmospheric contribution to these spectra, and the synthetic transmission spectra provided the specific form of that contribution. The spectral region across the two unsaturated water bands centered near 0.94μm and 1.13μm was assumed to represent the amount of atmospheric water vapor affecting the field data; the synthetic transmission spectra were fitted to the raw data in this spectral region and then used to extrapolate the atmospheric contribution to longer wavelengths, encompassing saturated water-vapor absorption bands.

In order to bring the raw and synthetic spectral dats sets into a comparable form two initial calibrations were necessary: the removal of the solar spectrum and of the spectrophotometer system's response curve, two wavelength dependent functions not present in the LOWTRAN-generated transmission spectra. A basic difficulty in analyzing remote spectroscopic data has been the separation of atmospheric absorption effects from surface (geologic) absorption. Under this research a unique and workable solution to this problem was developed: it was found that the temporary removal from the raw spectrum of a suitably defined continuum factored out, to a substantial extent, large-scale effects on the remote spectrum of absorption by the objects under analysis, thus isolating the atmospheric contribu-

tion to the raw data. A similarly defined continuum, representing to a rough approximation the aerosol contribution to atmospheric scattering, was removed from the synthetic transmission spectrum, bringing the two data sets into comparable form.

An iterative procedure was developed for comparing these two data sets; the iteration was based upon the amount of water vapor (in terms of density) assumed to be present in the bottom three layers of the LOWTRAN model atmosphere when forming the synthetic spectra. A set of synthetic transmission spectra was generated, each member having a different water-vapor density configuration for the lower atmospheric layers. The determination as to which synthetic spectrum was most representative of the atmospheric contribution to a given raw spectrum was based upon the closeness-of-fit between the synthetic spectrum and the raw spectrum at the bottoms of the two unsaturated water-vapor absorptions centered near $0.94\mu m$ and $1.13\mu m$. After the best-fit synthetic transmission spectrum was obtained from the set of synthetic spectra, the water vapor density of the bottom three layers was iteratively altered, and the closeness-of-fit test repeated, until a synthetic atmospheric transmission spectrum was obtained for which the difference in the average band depths (of these two unsaturated water-vapor absorption bands) between the raw and synthetic spectra was zero to several decimal places. This synthetic transmission spectrum was then divided out of the raw field spectrum as representing the atmospheric contribution to the remotely-obtained data. Finally, the continua defined earlier for

the raw field spectra were factored back in to reintroduce the spectral features of the geologic surface, and the mineralogical information contained therein.

CONCLUSIONS

The ultimate test of how well the synthetic transmission spectra represent the atmospheric absorptions present in the object data is the comparison of the calibrated remotely-obtained data to laboratory-obtained spectra for the same object. In general the agreement between calibrated field data and laboratory spectra is excellent for the wavelength region short of the saturated water-vapor band near 1.4μm, which was also the region used for testing the goodness-of-fit between the raw field spectra and the synthetic transmission spectra. The 1-μm olivine and pyroxene crystal-field absorption bands present in the spectra for the two basalt samples were very well preserved with the calibration procedure. The overall shape of the spectra for these two samples was also well-preserved across the entire spectral region. For the other two samples, the general spectral shape was highly similar for both the laboratory and field data of the white reflectance standard; it was only slightly similar for the carbonate sample longwards of the region used to test the goodness-of-fit. In both these samples many of the absorption features present in the laboratory data do not appear in the field data, as they are coincident with one or both of the saturated water-vapor bands centered near 1.4μm and 1.9μm. It is expected that further refinements in the technique will improve the calibration in the wavelength region longwards of the 1.4μm water-vapor band.

The above comparisons demonstrate the effectiveness of the calibration technique developed in this research. In most cases, useful mineralogical information contained in the remotely-sensed near-infrared data was successfully extracted from the raw (atmosphere-affected) data and enhanced through the calibration process--without reference to an external calibration standard. In the future this technique will be expanded and refined to be practically applicable to high spectral resolution image data such as will be obtained from mapping (imaging) spectrometers.

REFERENCES

Kneizys, F.X., E.P. Shettle, W.O. Gallery, J.H. Chetwynd, Jr,
L.W. Abreu, J.E.A. Selby, R.W. Fenn, and R.A. McClatchey (1980),
Atmospheric Transmittance/Radiance: Computer Code LOWTRAN 5,
AFCRL Environmental Research paper, No.697, AFCRL-80-0067.

McClatchey, R.A., R.W. Fenn, J.E.A. Selby, F.E. Volz and J.S.
Garing (1972), Optical Properties of the Atmosphere (3rd ed).
AFCRL Environmental Research Paper, No.411, AFCRL-72-0497.

TABLE OF CONTENTS

LIST OF TABLES

LIST OF FIGURES

CHAPTER I

BACKGROUND

A. INTRODUCTION

Remotely-sensed spectral data of the earth's surface derived from any instrument--whether photographic camera or multispectral mapper--necessarily contain the effects of absorption and scattering due to the earth's atmosphere. Unless these data are properly calibrated, and corrections made for atmospheric effects, spectral signatures may be so altered by the atmosphere that quantitative (and often even qualitative) comparisons of remotely-obtained data may be impossible, thereby precluding any compositional analysis. The primary objective of this research was to develop an analytical technique for removing these absorption and scattering effects. The approach taken has been to use the actual remotely-measured near-infrared spectral data as the basic "sounding mechanism" to describe the atmospheric effects, and to combine this information with transmission spectra obtained from a modified version of an existing atmospheric model (called LOWTRAN, McClatchey et al., 1972) in order, then, to calibrate the near-infrared spectral data.

The method proposed for this research offers a unique way in which the remote spectra may, in themselves, be used to provide an estimate of atmospheric conditions. Thus, atmospheric data are obtained at exactly the same time as target data and, therefore, simultaneity of acquisition is inherent. However, under this proposed technique, atmosphere and target data are not separate measurements and thus a new requirement arises: Separating the desired target data from the atmospheric data (or separating desired signal from undesired signal). The technique for performing this deconvolution requires high-resolution ($\delta\lambda/\lambda$ ~2-3%)

spectral data, such as may be obtained in the form of single-point spec-
tra from a spectrophotometer or, ultimately, in the form of three-
dimensional data from a mapping spectrometer.

The past fifteen years have seen a rapid development of remote
sensing techniques and in the applications of these techniques to geo-
logical problems. Although the photographic camera is still a widely
used and valuable sensor, other more sophisticated instruments are now
in routine use as well. While a number of air- and space-borne sensors
have been flown (e.g. Goetz et al. 1975), the most influential of these
experiments in demonstrating the utility of remote sensing as a geologi-
cal tool has undoubtedly been the Landsat series of satellite-borne mul-
tispectral scanners (MSS). Four of these satellites have been launched,
beginning with Landsat-1 in July 1972, and the most recent, Landsat-4
(launched in August 1982), also has on board an instrument, the Thematic
Mapper, which is responsive in selected bands in the near- to mid-
infrared (1.0μm - 14.0μm) regions of the electromagnetic spectrum.
Instruments such as the TM promise to be a significant improvement over
previous earth orbital sensor systems for characterizing geological
materials. Unfortunately, the Thematic Mapper operated for only about
four months before control was lost and although this turned out to be a
problem in data transmission, the solar panels are presently in danger
of failing, which would make the entire instrument inoperable. However,
the replacement instrument for the Thematic Mapper, Landsat D' is
scheduled to be launched in early 1984.

The Landsat multispectral scanners collect data through wide-band
wavelength filters; the spectral resolution of the images obtained is
limited by the width of these bands. For the Thematic Mapper filters,
the bands range in width from about 0.06-0.36 μm in the visible and

- 2 -

near-infrared to 2.1 μm in the mid-infrared. While Landsat 4 is an improvement over earlier spacecraft in the series (both spatial and spectral resolution are improved), it still carries only seven filters.

In addition to the Landsat 4 Thematic Mappper, advanced forms of airborne multispectral instruments have been developed. One type of instrument, the mapping spectrometer, obtains spatial data at many continuous, closely spaced wavelengths. The data output from a mapping spectrometer can be thought of as of images (two dimensions along a ground-track) obtained at very close wavelength intervals, or as full spectra for each spatial pixel: a three-dimensional data set. Methods for manipulating the large quantity of data which will result from such instruments are currently under development. It is intended that the technique developed in this research for removing atmospheric effects from near-infrared spectral data will be applicable, with some modification, to mapping spectrometer data. The means by which this application may be effected are discussed in later chapters.

B. DETERMINATION OF REFLECTANCE

In order to convert the brightness (or spectral "radiance"; Slater, 1980) of the surface as measured by the spacecraft into a form which is comparable to laboratory data, it is necessary to account for the varying spectral irradiance (resulting from scattering and adjacency effects) inherent in the scene and so derive the spectral reflectance of the surface. To convert remotely-measured radiance values to their reflectance equivalents, two corrections must be made to the data: 1) A correction for the sun and sky irradiance at the earth's surface; and 2) A correction for the absorbing and scattering effects of the atmosphere.

Before considering the various methods which have been utilized for this calibration of remotely-sensed data, it is useful to examine the methods used for calibrating comparable laboratory and astronomical data to an absolute reflectance.

1. Calibration of Laboratory Data

In the case of laboratory spectra, the calibration process is much simpler than for remotely-sensed data. Because of the very short path length from the light source to the object to the sensor, atmospheric effects are far less severe than in field data. The problem of calibration under laboratory conditions reduces to the identification of a suitably bright and constant standard of well-known spectral reflectance for use as the scale for absolute reflectance. The two standards most commonly employed are MgO and Halon (Venable et al, 1976), both of which have been calibrated by the National Bureau of Standards. In order to remove the effects of system variability and random low-level light fluctuations, a dark threshold signal level is also measured and subtracted from the measured signals of both the object and the white standard. The full calibration is performed by applying the following equation (Eqn. 3.1):

$$\frac{F_{(obj)} - F_{(dark)}}{F_{(halon)} - F_{(dark)}} \; * \; R_{(NBS.halon)} \quad ;$$

where $F_{(obj)}$ is the measured flux or signal of the object of interest, $F_{(dark)}$ is the measured flux of an unilluminated sample, $F_{(halon)}$ is the measured flux of the chosen white standard, and $R_{(NBS.halon)}$ is the National Bureau of Standards published reflectance for the Halon.

- 4 -

2. Calibration of Astronomical Data

In the case of astronomical data, calibration is made with respect to some set of standard sources: typically an area of the moon (the Apollo 16 landing site) or one of several bright stars in the same region of the sky, which consequently has the same air mass range as the object under observation (McCord and Clark, 1979). These standard sources may then be referenced to laboratory standards through comparison with a bright star which has an identified solar-like spectrum (and thus to a comparison of the spectrum of a laboratory standard under solar illumination) or, alternatively, other sources may be used to establish the "absolute" reflectance of the standard star(s). The "extinction technique" for using these standard star observations to remove atmospheric effects in near-infrared data is discussed in detail in McCord and Clark (1979). Given the relatively low total mass of the atmospheric column over Mauna Kea (where McCord and Clark's measurements were made) as well as the constancy of the atmosphere over Mauna Kea when observations were made, they conclude that with frequent reference to the standard sources, telluric atmospheric absorption effects (principally water) may, under ideal conditions, be completely removed from astronomical data.

Neither of these two factors--the constancy or rarity of the atmosphere--will hold true when observing the earth's surface from an aircraft or satellite. Even at Mauna Kea, atmospheric conditions are considered to be "photometric" for only about 70% or less of the potentially available observing time (pers.comm., R.H. Brown, 1983). Under typical terrestrial remote-sensing conditions where there is a long

and, more critically, variable atmospheric path length, astronomical calibration techniques are inadequate. The purpose of this thesis is to explore an approach to the problem of making atmospheric corrections to remotely sensed spectral data under terrestrial conditions. The goal is to define a method of performing atmospheric calibrations so as to circumvent the problem of temporal and spatial variability of the atmosphere over the target; this method will then be applied to a terrestrial data set.

C. THEORY AND PRACTICE OF FIELD CALIBRATION

To obtain a calibrated reflectance spectrum of an object on the earth's surface, the quantities which must be measured or estimated are:

$E(\lambda)$, the surface spectral irradiance, which is:

> the sum of the direct solar flux incident on the surface, per unit area of surface, and the diffuse, or scattered, atmospheric flux incident on the surface, per unit area of surface. (This quantity is hereinafter referred to as surface irradiance.);

$\tau(\lambda)$, the atmospheric spectral transmittance; or

$\tau(\lambda, ext)$, the spectral extinction optical thickness

$$= (\tau = e^{(-\tau(ext))});$$

$L(\lambda)$, the upwelling, atmospheric-path spectral radiance from the ground to the sensor (i.e., the spectral radiant flux coming from the target, hereinafter called target radiance); and

$S(\lambda)$, the upwelling radiance scattered into the line-of-sight by the atmosphere.

The inter-relationships between these parameters (all of which are a function of wavelength, λ) will be considered in detail in chapter two; at this point, however, it is pertinent to review field calibration techniques utilized in the past. The various approaches may be subdivided either with reference to the calibration technique itself or with reference to the type of data to which the calibration technique has been applied. In the following discussion, three subclasses of technique are discussed: 1) Calibration with reference to laboratory-calibrated standard; 2) Calibration using a portion of the target as a reference standard; and 3) Calibration making explicit use of measured or estimated atmospheric parameters. In general, the first of these has been primarily applied to the analysis of comparatively high-resolution spectroscopic data (with the exception of the work of McDowell and Specht (1974) in photographic film densities to spectral reflectance), the second has been applied to both high-resolution and broadband spectroscopic data, and the third has only been used in the analysis of broadband imagery and photographic film. The technique developed in the present research may be put most readily into the latter category, in that the LOWTRAN-produced synthetic atmospheric transmission spectra are used to explicitely represent the atmospheric component to the high-resolution near-infrared spectral data, without reference to any additional standard.

1. Calibration With Reference to a Laboratory-Calibrated Standard

Several methods have been proposed by which the surface irradiance, the extinction optical thickness and the target radiance (i.e., the parameters of concern here) may be implicitly accounted for. Such methods make reference to observations of an object (or area) of known reflectance which is both temporally and spatially close to the object

of interest. This standard is used in the calibration process in much
the same way that the aforementioned laboratory white standard is used
to calibrate laboratory data. In order for this field reference tech-
nique to be effective, both atmospheric and irradiance conditions
between the object and the sensor, and between the standard and the sen-
sor, must be essentially the same. If there are unknown lateral or tem-
poral inhomogeneities in the atmosphere, errors in calibration will
result. Because of the difficulties of erecting a calibrated reflec-
tance standard near the target being remotely measured, this technique
has been most successfully applied to high-resolution spectroscopic
data, rather than to broadband spectra or imagery.

a. Goetz et al. (1975)

A procedure very similar to that commonly used in the laboratory
was followed by Goetz et al. (1975) to calibrate field spectra obtained
in Nevada with their portable field reflectance spectrometer (PFRS).
Using this radiometer, which was designed and built at the Jet Propul-
sion Laboratory (JPL), radiance data were collected of an object at a
distance of about 1 meter from the sensor; frequent measurements of the
white reflectance standard (a material called FibreFax, calibrated to
laboratory standards) were interspersed with the object measurements.
Examples of spectra obtained and calibrated by Rowan et al. (1977)
using this scheme are shown in Figure 1.1; it is important to note that
even over this very short horizontal path length the distance from sun
to object is still quite long and, thus, the two atmospheric absorption
bands at 1.4μm and 1.9μm, corresponding to the absorption frequency of
water molecules in the atmosphere, are fully saturated, so that informa-
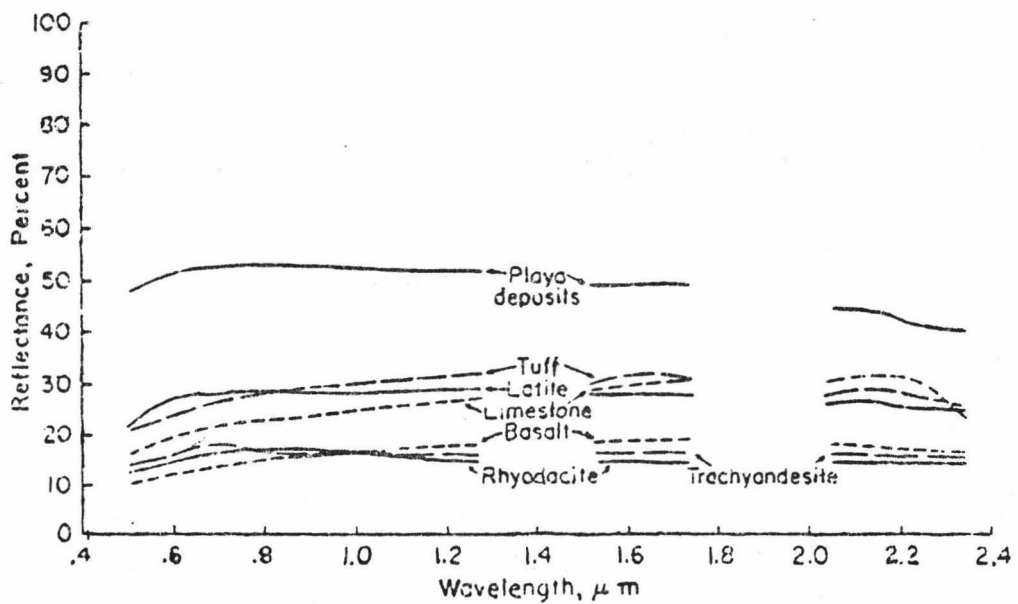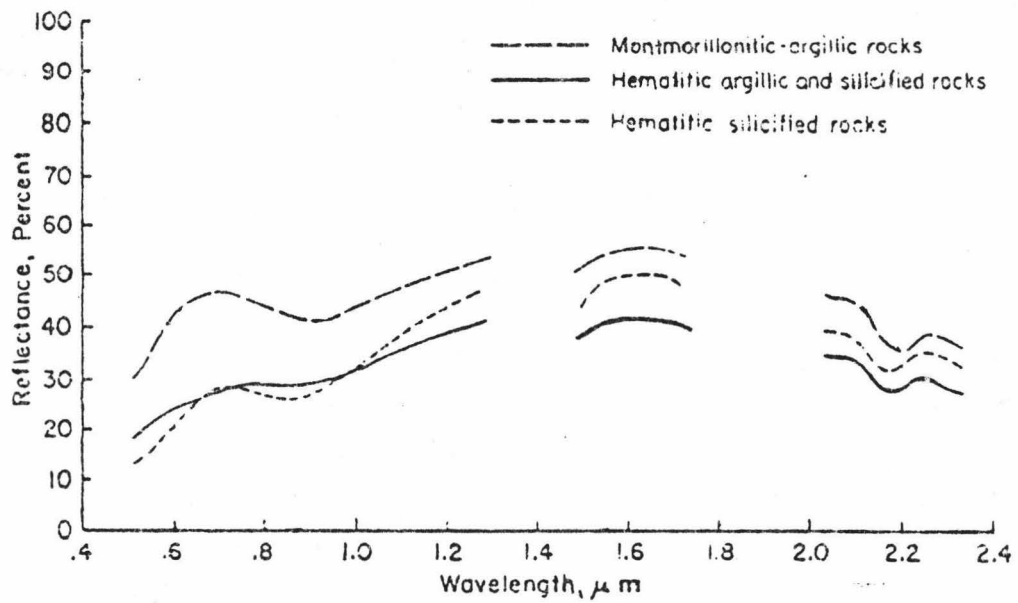tion regarding spectral reflectance is masked.

Figure 1.1

Field Reflectance Spectra obtained by Rowan et al. Using the JPL PFRS
(Portable Field Reflectance Spectrometer) (from Rowan et al., 1977, p.525)

b. Singer et al (1981)

A comparable method was employed by Singer et al. (1981) in a project which used remotely-acquired near-infrared spectral data to analyze the wall stratigraphy of Kilauea caldera on Hawaii. In this case, the caldera wall was observed from the opposite side of the caldera, a distance of about three kilometers; calibration was done using both a white and a black standard, which were erected on the caldera rim above the strata being analyzed. The black standard was used in an analagous way to the threshold dark in the laboratory, in order to calibrate the effects of atmospheric scatter and variation in instrument response. The white standard was a painted surface which had been calibrated to laboratory standards. With the combination of these two standards, it was hoped that calibration to absolute reflectance could be performed. The particular locale chosen as a test site for the method proved to be especially troublesome, owing to the highly variable atmospheric absorptions caused by fumerole activity within the caldera; accurate calibration of these data was therefore not possible because of these rapid temporal and spatial changes.

The technique of Singer et al. was employed again in 1982 (Singer et al., 1984) over a shorter distance (about 0.5 kilometer, at sealevel) across a more constant atmospheric path to obtain remote measurements of laboratory-calibrated samples. Spectra resulting from this test are shown as Figure 1.2a-c along with their laboratory-obtained counterparts; it is apparent that while the calibration is good, laboratory and field spectra are not identical. The probable reasons for this discrepancy are two-fold: 1) The different viewing geometries in the laboratory and the field; and 2) The different sized areas over which the sample integration was performed. The viewing geometry used in the
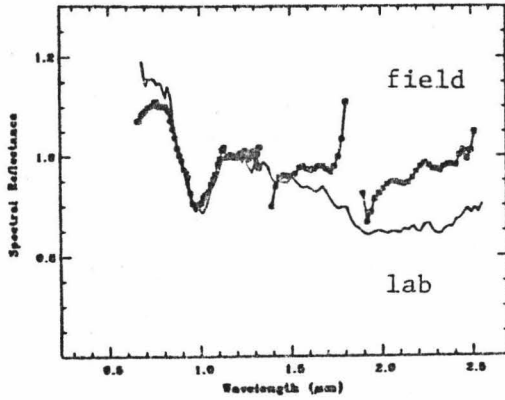
a. Nepheline Basalt
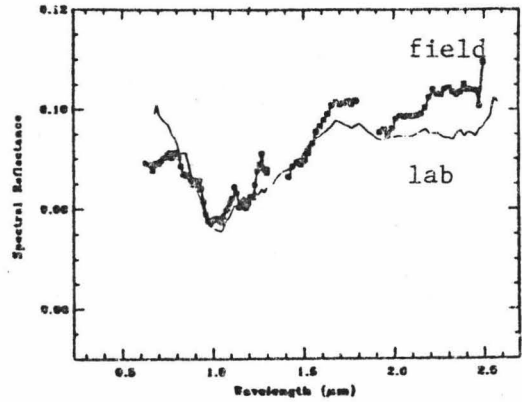
b. Olivine Basalt
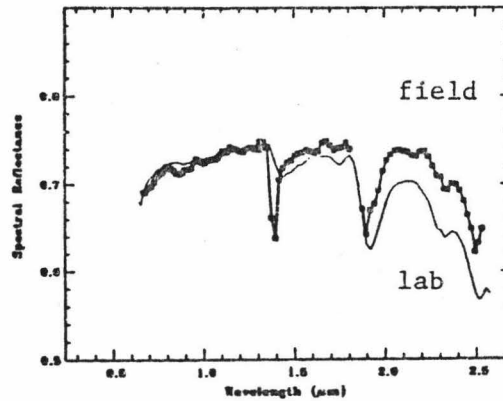
c. Carbonate

Figure 1.2

Field Reflectance Spectra Obtained by Singer et al. Using the Planetary
Geosciences Division CVF spectrophotometer (Singer et al, 1982, unpub.data)

laboratory can only be an approximation to that existing in the field; likewise the sample selected and analyzed in the laboratory can only approximate the bulk material measured in the field. That these differences are not problems of the calibration technique per se is evident from the fact that samples having similar reflectances do not necessarily have similar deviations from their laboratory-obtained reflectances, as would be expected from a poor calibration to absolute. A poor atmospheric calibration would be evident in the field spectra by incompletely removed water absorption features, and in particularly by a negative slope towards the infrared portion of the spectrum owing to incomplete removal of the effects of the massive water absorption feature near 2.7μm; these diagnostics are not apparent in the field spectra, but corrections for atmospheric water were still not perfect.

c. McDowell and Specht (1974)

Similar methodology has also been followed in work conducted by McDowell and Specht (1974) in order to relate photographic film densities to the spectral reflectance of an area. They found that, through a suitable transformation of the three principal characteristic vectors obtained in a multi-variate principal components analysis, radiances of field crops as recorded on film could be related to the spectral response through a red, a blue and a green filter. In order to calibrate their data to absolute standards, they included in their photos an asphalt road (to remove the varying scene irradiance) and a white standard, which they devised specifically for the calibration of field data to absolute reflectance in the laboratory. Their photographic data were obtained from an altitude of about 1500 meters and the corresponding calibration data from a distance of about 2 meters. The application of this calibration technique depends upon the consistency of the film

response between calibrations, although they obtained errors on the order of 10% for the study reported.

2. Calibration Using Portion of Target as Reflectance Standard

The chief drawback to any method which relies solely on making frequent references to well-calibrated standards is the obvious: The standards must be available throughout the scene and must be large enough to be resolvable by the sensor. Furthermore, atmospheric conditions and the atmospheric path-length from sensor to standard must be sufficiently comparable to the conditions and path length from the sensor to the object or area being studied. These two conditions may be difficult or effectively impossible to meet on an operational basis, especially in observations of large and/or remote areas. Unfortunately, these are just the areas to which remote sensing methods might be most logically applied. Therefore, an extension of the technique of using a laboratory-calibrated standard was developed; this extension utilizes some material within the scene as the standard of reflectance.

a. Goetz et al (1982)

The latter situation was the case in the Shuttle Mapping Infra-Red Radiometer (SMIRR) experiment conducted by Goetz et al. (1982). The filter band passes used in this instrument (some quite narrow) were selected in order to avoid the worst regions of atmospheric absorption (shown in Figure 1.3a). The data were obtained from an altitude of about 262 kilometers across the regions shown in Figure 1.3b. Because of the uncertainty of the actual flight path prior to the mission, and because of the large areas being covered, it would have been impractical to erect sufficiently large standards along the groundtrack to calibrate the data. Instead, ground samples were taken after the flight of a bright area identified along the groundtrack in the particular test
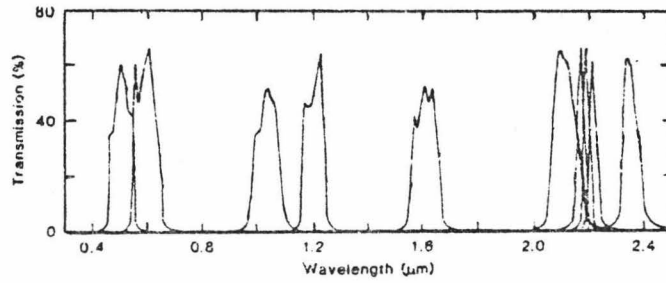
Figure 1.3a

Bandpasses for the 10 SMIRR (Shuttle Mapping Infrared Radiometer)

Spectral Filters (from Goetz et al, 1982, p.1021)

Figure 1.3b

Groundtrack for SMIRR Flight Coverage, November, 1981

(from Goetz et al, 1982, p.1021)

region (in Egypt) being analyzed; these hand samples were measured against laboratory standards. SMIRR spectra obtained of this bright area were then used to calibrate other spectra taken during the flight. Regions of deep shadow were assumed to be returning a surface reflectance signal only indirectly, through the scattering properties of the atmosphere, and therefore were used as dark standards to remove the effects of scene irradiance. This sort of calibration scheme can be successful only to the extent that the laboratory measurements and the samples collected successfully simulate field conditions, especially atmospheric conditions. The atmosphere over the region studied is quite dry, and relatively homogenous both laterally and temporally; the calibration scheme employed would be considerably less successful if this were not the case, since the area used as a calibrator represents only a small region across the scene being examined, as well as only a limited sample of the atmospheric path.

b. Collins et al (1981)

Collins et al. (1981) used an area in a particular region in Nevada, for which they obtained spectral data, as an indirect calibrator. They did not, however, calibrate their radiometer data to this region (a dry lake bed), but simply used spectra of the lake bed for visual and qualitative comparison against other remotely-obtained spectra. They made no attempt beyond this to remove the effects of the atmosphere or of the solar spectrum (as different from laboratory illumination) from their data.

3. Calibration Using Measured or Estimated Atmospheric
   Parameters Directly

As with calibration methods which make use of a standard erected on-site, techniques using a natural surface as a standard require that

the calibration observations are made at or near to the same time as remote observations of the object. Several schemes have been developed in attempts to avoid this constraint; these are directed towards obtaining explicit values for the surface irradiance and beam transmittance effective over a given region, and then using these values in conjunction with remotely-obtained radiance values to obtain the target radiance and, thus, the calibrated reflectance. Such schemes tend to require more elaborate measurements, specific to a given site, than the methods described above; their chief advantage is that they allow for some latitude in the timing involved in acquiring calibration measurements. The inherent variation in the atmosphere over a region introduces an inherent error into any such estimates of atmospheric parameters; for this reason, primarily, these methods have been most successfuly applied to broadband spectral data.

a. Otterman et al (1980)

Such a method was tried by Otterman et al. (1980), who divided the upwelling path (or target) radiance, $L(\lambda)$, into three (wavelength-dependent) components:

1) $L(\lambda r)$, the radiance reflected from the target that, although attenuated by the atmosphere, reaches the sensor;

2) $L(\lambda a)$, the radiance reflected from the surface in the general vicinity of the target that reaches the sensor by being scattered by the atmospheric column above the target; and

3) $L(\lambda d)$, the radiance reaching the sensor that has been scattered from the direct solar beam.

The target radiance may then be obtained from these three components by the relationship:

$$L(\lambda) = (L(\lambda r) + L(\lambda a) + L (\lambda d)) * \pi/\mu_0 ;$$

where μ_0 is the cosine of the zenith angle.

Expressions were developed for the three components of radiance from a "simplified single scattering" treatment of radiative transfer. Owing to the approximations inherent in this approach, the formulae developed are only valid for cases of low optical thickness; that is, where the sum of the backward-scattering optical thickness, B, the absorption optical thickness, W, and the forward-scattering optical thickness, F, all divided by μ_0, is less than 0.1 (or: $(B+W+F)/\mu_0 < 0.1$). Also, because of simplifications which they made for the aerosol phase function, the formulae are only valid for small zenith angles ($<65°$). They also assume a cloud-free, planar, and horizontally uniform atmosphere.

Otterman et al. applied their expression for $L(\lambda)$ to correct Landsat data for atmospheric effects. Their primary conclusion was that only two atmospheric parameters affect the radiance measurements. These are B and W, the backscattering optical thickness and the absorption optical thickness, given above. They further concluded that adjacency effects must be considered when large uniform surfaces cannot be assumed as the target. This requires consideration of an additional atmospheric parameter, F, the forward scattering optical thickness, in order to describe cross-radiance (adjacency) effects.

In application, Otterman et al. found the accuracy achieved with this technique to be on the order of $(B+W+F)/\mu_0$ (<0.1). This describes

the error which is inherent within the technique and does not include error in measuring or estimating B, W, or F, which may, of course, be large.

b. Gordon et al (1973) and Rogers and Peacock (1973)

Gordon et al. (1973), using Duntley's (1948) concept of equilibrium radiance, developed a method for determining the atmospheric-path (or target) radiance using ground-based measurements of beam transmittance and surface irradiance. Their particular application was to obtain calibrated contrast transmittance from airborne photographic data; Rogers and Peacock (1973) used essentially the same technique to calibrate Landsat data. Gordon's method made use of the equilibrium radiance to arrive at the following expression for the upwelling-path (or target) radiance:

$$L(\lambda) = L(\lambda h)*(1-\tau(\lambda)/(1-\tau(\lambda h))),$$

where $L(\lambda h)$ is the radiance across a horizontal path, τ is the ground-to-space optical thickness, and $\tau(\lambda h)$ is the horizontal optical thickness. All of these variables are functions of wavelength. Of these values only $L(\lambda)$ is unknown; $L(\lambda h)$ is obtained by approximating the equilibrium radiance for a set of standard atmospheric conditions (an approximation which Gordon et al. (1973) showe to be valid), τ is computed from the ground with a solar radiometer measuring center-sun radiance, and $\tau(\lambda h)$ is determined using the Langley-plot method. This latter method makes use of the fact that there exists a predictable relationship between spectral irradiance and zenith angle as measured for a given area for different values of the extinction coefficient. Clearly the limiting factors to this technique are the availability of

the above information for an area being studied as well as the closeness of the "standard atmosphere" to prevailing atmospheric conditions. The technique provides reliable estimates of reflection, however; Rogers and Peacock (1973) estimated errors of $\pm$ 5% using a portable radiometer and this method to calibrate Landsat data.

c. Dana (1975, 1978)

Dana (1975 and 1978) used a related method to obtain reflectance; however, instead of extensive ground-based atmospheric data, low-altitude aircraft measurements were employed (although ground-based measurements could also be used) to provide the ground-truth for calibration of Landsat radiance data. Dana employed a linear atmospheric model relating remotely-measured radiance to surface reflectance. The basic linear model has the form:

$$E(\lambda s) = E(\lambda) * \tau * R/\pi + L(\lambda) \qquad ;$$

where $E(\lambda s)$ is the sensor-acquired radiance, $E(\lambda)$ is the surface irradiance, τ is the ground-to-sensor optical thickness, R is the terrain reflectance, and $L(\lambda)$ is the upwelling path radiance, all of which are functions of wavelength, λ. For very low-altitude measurements, where the effects of atmospheric path are assumed to be minimal, this becomes:

$$E(\lambda a) = E(\lambda) * R/\pi \qquad ;$$

where $E(\lambda a)$ is the low-altitude-acquired radiance and the other variables are as above. Instruments on board the aircraft measure $E(\lambda a)$ and $E(\lambda)$ and so R can be determined for specific training sites. These values of R, preferably for areas with large differences in brightness,

are then used in the linear model equation to determine τ and $L(\lambda)$. As long as the atmosphere can be presumed to remain constant over the region being studied, then this linear fit can be used to calibrate radiances for the objects of interest. Using this model, Dana obtained correlation coefficients (R^2) >0.94 for the linear fit.

d. Piech and Walker (1974)

Techniques which use an area in the scene to obtain calibration to absolute values require a certain atmospheric homogeneity across the scene. Inhomogeneities represent the chief limitation to any method utilizing a specific area or material for calibration or ground-truth, but there are methods which at least partially circumvent this limitation (Piech and Walker, 1974). Utilizing shadows across areas within the observed scene as the basic element of calibration, Piech and Walker coupled the measurements with occasional reference to some in-scene standard to obtain absolute calibration. The technique used a linear model relating the radiance of an unshadowed area in the scene, $E(\lambda u)$ (adopting the notation of Slater, 1980), to the radiance of the same area in shadow, $E(\lambda s)$. This straight-line fit has a slope of $E(\lambda s)/E(\lambda u)$, where $E(\lambda s)$ and $E(\lambda u)$ are the irradiances due to the sky alone and to the sun and sky, respectively. The intercept of this line is $b=\pi*L(\lambda u)*(1-E(\lambda s)/E(\lambda u))$. Since the slope and intercept are both known, $L(\lambda u)$, the upwelling path radiance can be determined. If the total surface irradiance, $E(\lambda u)$, and the extinction coefficient, τ, are determined with reference to some known area in the scene (Piech and Walker used asphalt roadways), then the reflectance, R, can be obtained

with the same basic equation as used by Dana above (again, all of the variables are wavelength-dependent):

$$E(\lambda u) = E(\lambda u) * R * \tau/\pi + L(\lambda u).$$

Each of the techniques described above utilizes an atmospheric correction scheme which requires some estimate of, or surrogate for, atmospheric conditions at the time of obtaining the remote data. The degree of success in removing atmospheric effects from the data is the same as the degree of knowledge of atmospheric conditions. When these conditions are measured or estimated (as with the use of a "standard atmosphere"), the degree of success is related to the accuracy of these estimates. When a surrogate (such as a white, calibrated standard) is used, the degree of success is dependent upon the spatial and temporal proximity of this surrogate to the target of interest. In all cases, the ultimate limiting factor is the degree to which atmospheric data may be simultaneously acquired with target data.

D. REFERENCES

Collins, W., Chang, S., and Kuo, J.T. (1981). "Remote Mineralogical Analysis Using a High-Resolution Airborne Spectroradiometer: Preliminary Results of the Mark II System", in 1981 International Geoscience and Remote Sensing Symposium (IGARSS'81) Digest, 1 :337-344.

Dana, R.W. (1975). "Solar and Atmospheric Effects on Satellite Imagery Derived from Aircraft Reflectance Measurements", in Proc. of the 10th International Symposium on Remote Sensing of Environment, 2 :683-694.

Dana, R.W. (1978). "Using Airborne Radiometry to Determine Atmospheric Effects in Landsat Data", Am. Soc. Photogram., Fall Technical Meeting.

Duntley, S.Q. (1948). "The Reduction of Apparent Contrast by the Atmosphere", J. Opt. Soc. Am., 38 :179-185.

Goetz, A.F.H., F.C. Billingsley, A.R. Gillespie, M.J. Abrams, and Squires, R.L. (1975). "Application of ERTS Images and Image Processing to Regional Geologic Problems and Geological Mapping in Northern Arizona", NASA Type III Report, NASA-CR-143068.

Goetz, A.F.H., Rowan, L.C., and Kingston, M.J. (1982). "Mineral Identification from Orbit: Initial Results from the Shuttle Multispectral Infrared Radiometer", Science, 218 :1020-1024.

Gordon, J.I., Harris, J.L.,Sr, and Duntley, S.Q. (1973). "Measuring Earth to Space Contrast Transmittance from Ground Stations", Applied Optics, 12 (6):1317-1324.

McClatchey, R.A., R.W. Fenn, J.E.A. Selby, F.E. Volz and J.S. Garing (1972), Optical properties of the Atmosphere (3rd ed). AFCRL Environmental Research paper, no.411, AFCRL-72-0497.

McCord, T.B. and R.N. Clark (1979). "Atmospheric Extinction 0.65-2.50μm Above Mauna Kea", _Publ. of the Astron. Soc. of the Pacific_, _91_ :571-576.

McDowell, D.Q. and Specht, M.R. (1974). "Determination of Reflectance Using Aerial Photographs", _Photogrammetric Engineering_, _40_ :559-568.

Otterman, J., S. Unger, Y. Kaufman and M. Podolok (1980), "Atmospheric Effects on Radiometric Imaging from Satellites under Low Optical Thickness conditions", _Rem.Sens.of Env._, _9_ :115-129.

Piech, K.R., and Walker, J.E. (1974). "Interpretation of Soils", _Photogram. Eng._, _40_ :87-94.

Rogers, R.H., and Peacock, K. (1973). "A Technique for Correcting ERTS Data for solar and Atmospheric Effects", in _Symposium on Significant Results of ERTS-1_, NASA SP-327.1115.

Roush, T.L., and Singer, Bob (1983) "Effects of Temperature on Mafic Absorption Features", in _Lunar and Planetary Science XIV Abstracts_, in Press.

Rowan, L.C., A.F.H. Goetz, and R.P. Ashley (1977), "Discrimination of Hydrothermally Altered and Unaltered Rocks in Visible and Near Infrared Multispectral Images, _Geophysics_, _42_ (3):522-535.

Singer, R.B., Blake, P.L., Lucey, P.G., and McCord, T.B. (1981). "Application of Reflectance Spectroscopy to Geologic Mapping on Earth: Stratigraphic Units in Kilauea Caldera", Annual Progress Report, JPL Contract #955722, Planetary Geosciences Division unpublished report.

Singer, R.B., Blake, P.L., Lucey, P.G., and McCord, T.B. (1984).
"Application of Reflectance Spectroscopy to Geologic Mapping on
Earth: Stratigraphic Units in Kilauea Caldera", Final Progress
Report, JPL Contract #955722, Planetary Geosciences Division unpub-
lished report.

Slater, P.N., (1980). Remote Sensing: Optics and Optical Systems,
Addison-Wesley Publishing Company, Reading, MA.

Venable, W.H., Jr., V.R. Weidner, and J.J. Hsia (1976), "Information
Sheet on Optical Properties of Pressed Halon Coatings", report,
Nat. Bur. of Stand., Washington, D.C.

CHAPTER II

THEORY AND MODELLING OF ATMOSPHERIC EFFECTS

A. INTRODUCTION

This chapter is devoted to providing background theory with regards to the processes of atmospheric absorption and scattering, as well as furnishing a description of the purpose, structure and use of the LOWTRAN model in the context of this study. It begins with a review of the basic physical processes involved in the atmospheric transmission and absorption of light; then discusses theoretical models designed to describe such radiative transfer; and concludes with a description of how these considerations are incorporated into the LOWTRAN computer model of the atmosphere.

B. ABSORPTION

The species responsible for atmospheric absorption generate a vast number of absorption lines. Seldom, however, are these lines observed individually; rather, it is the integrated effect of all the lines which is measured. The typical absorption spectrum of the combined atmospheric consituents is shown as Figure 2.1 ($20cm^{-1}$ resolution). This spectrum was obtained using the LOWTRAN model (Kneizys et al., 1980) discussed later in this chapter. Although oxygen and nitrogen are the most numerous species in the atmosphere (both by volume and mass percent), they, of themselves, contribute only negligibly to the absorption spectrum (Kondratyev, 1969, p.85). All of the main absorbing species, however, involve one or the other of these elements.
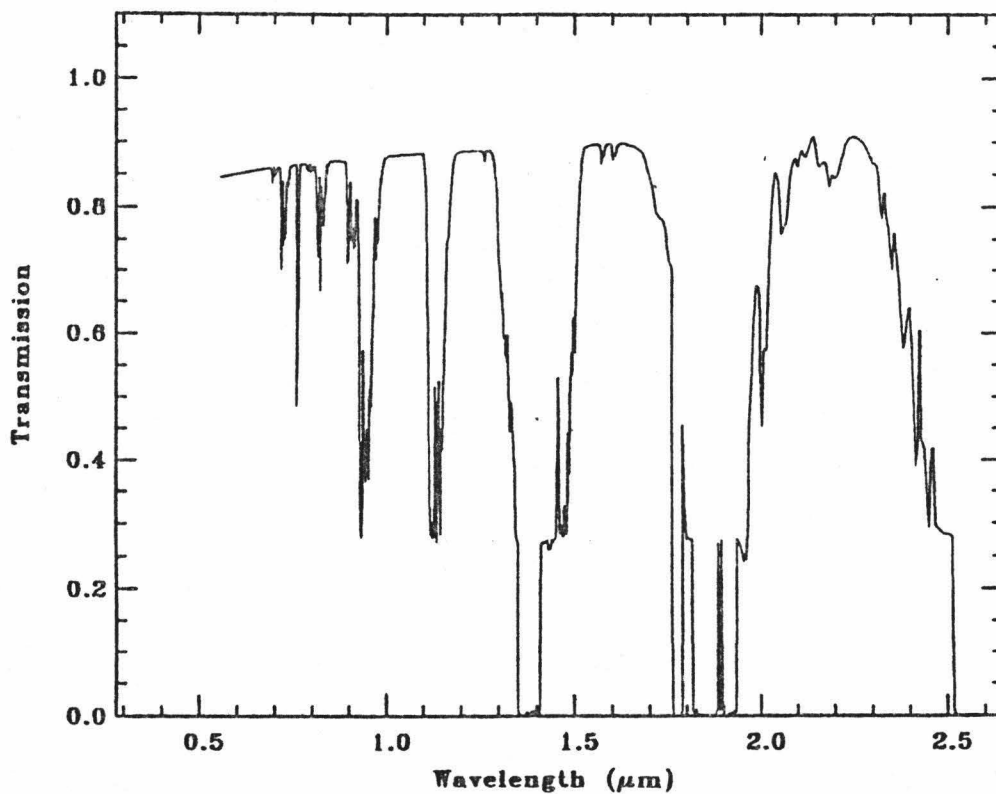
Figure 2.1

Atmospheric Transmission Spectrum Through a 1km Horizontal path
(20 cm^{-1} Resolution) (Calculated from LOWTRAN, Kneizys et
al., 1980)

1. Water Vapor

Water vapor (H_2O) is by far the single greatest contributor to the atmospheric absorption spectrum (Knodratyev, 1969, pp.107-122). The absorption spectrum of water vapor alone is shown in Figure 2.2. At the ultraviolet end of the spectrum, absorption by H_2O is the result of electronic transitions. In the wavelength region from 0.54 μm to 9.0 μm, absorption is the result of rotational-vibrational transitions and over-tones. In the far-infrared region, 9.0 μm to 1.5 cm, absorption is the result of strictly rotational transitions (Kondratyev, 1969, pp.108-109).

There are three normal vibrational modes of the water vapor molecule. These three vibrational modes have primary frequencies cen-tered at $v_1 = 3670$ cm^{-1} (2.72 μm), $v_2 = 1675$ cm^{-1} (5.97 μm), and $v_3 = 3790$ cm^{-1} (2.64 μm). The water vapor molecule also has three rotational modes. The results of these combined processes of vibration and rota-tion in the visible to near-infrared wavelength region are the broad absorption bands outlined in Table 2.1. Figure 2.3 shows the variation with absorption coefficient (in the form of band depth) as a function of the H_2O vapor density for the two bands centered (i.e. having maximum depth) at 0.935 μm and 1.13 μm.

2. Carbon Dioxide

The second most intense atmospheric absorber is the carbon dioxide molecule (CO_2)(Kondratyev, 1969, pp.123-131). Carbon dioxide does not exhibit absorption features in the visible portion of the spectrum, but does have several absorption features in the near- and mid-infrared regions (Figure 2.4). Since CO_2 is a linear molecule, all of these absorptions (summarized in Table 2.2) are the result of vibrational transitions.

Table 2.1

Water Vapor Absorption Bands

in the Near-Infrared Spectral Region

Spectral Region (μm)	Band Center (μm)
0.70 - 0.74	0.718
0.79 - 0.84	0.810
0.926 - 0.978	0.935
1.095 - 1.165	1.130
1.319 - 1.498	1.395
1.762 - 1.977	1.870
2.520 - 2.845	2.680

Source: Kondratyev, 1969, p.110

Table 2.2

Carbon Dioxide Absorption Bands

in the Near—Infrared Spectral Region

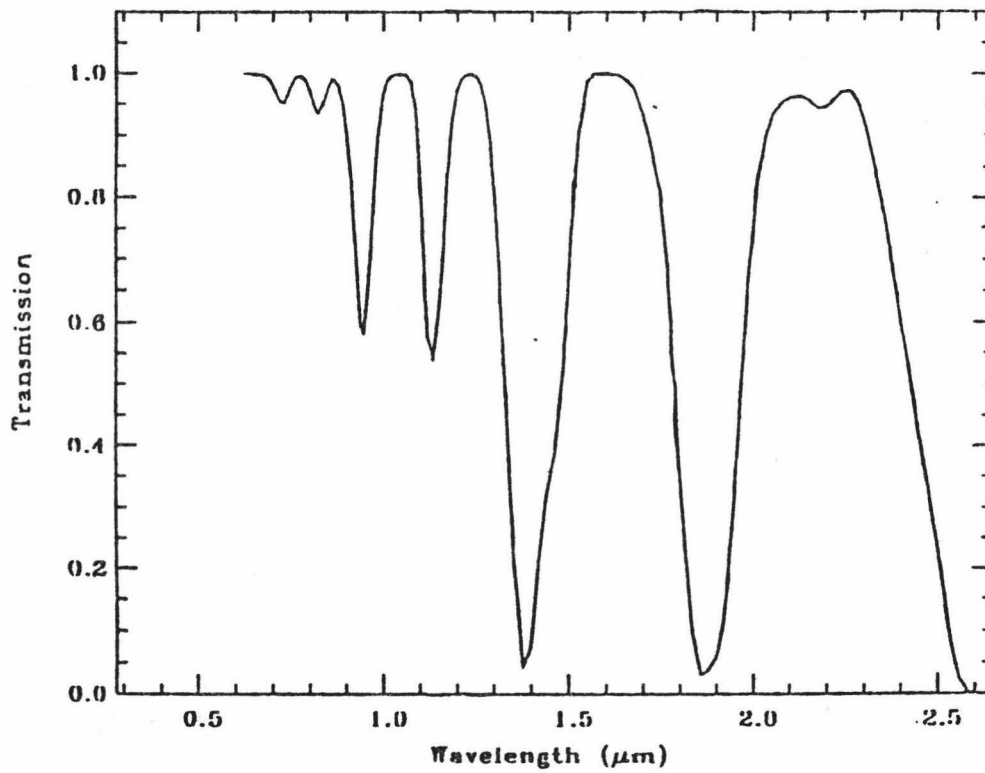| Spectral Region (μm)	Band Center (μm)
1.38 – 1.50	1.4
1.53 – 1.67	1.6
1.92 – 2.11	2.0
2.63 – 2.87	2.7
4.00 – 4.63	4.3
4.63 – 5.05	4.8
5.05 – 5.35	5.2
12.5 – 18.0	14.7

Source: Kondratyev, 1969, p.125

Figure 2.2

Water Vapor Transmission Spectrum Through a 1km Horizontal Path
(at CVF spectrophotometer wavelengths) (Calculated from LOWTRAN,
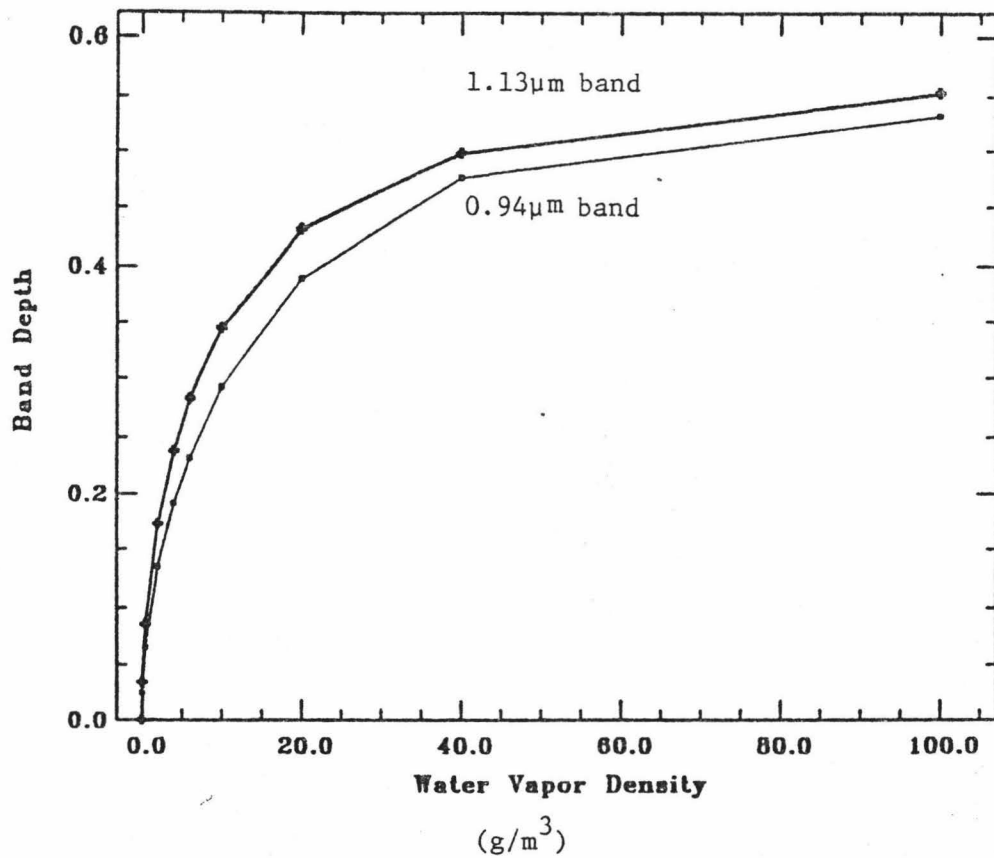Kneizys et al., 1980)

Figure 2.3

Band Depths of 0.94μm and 1.13μm Water Vapor Bands v.s.
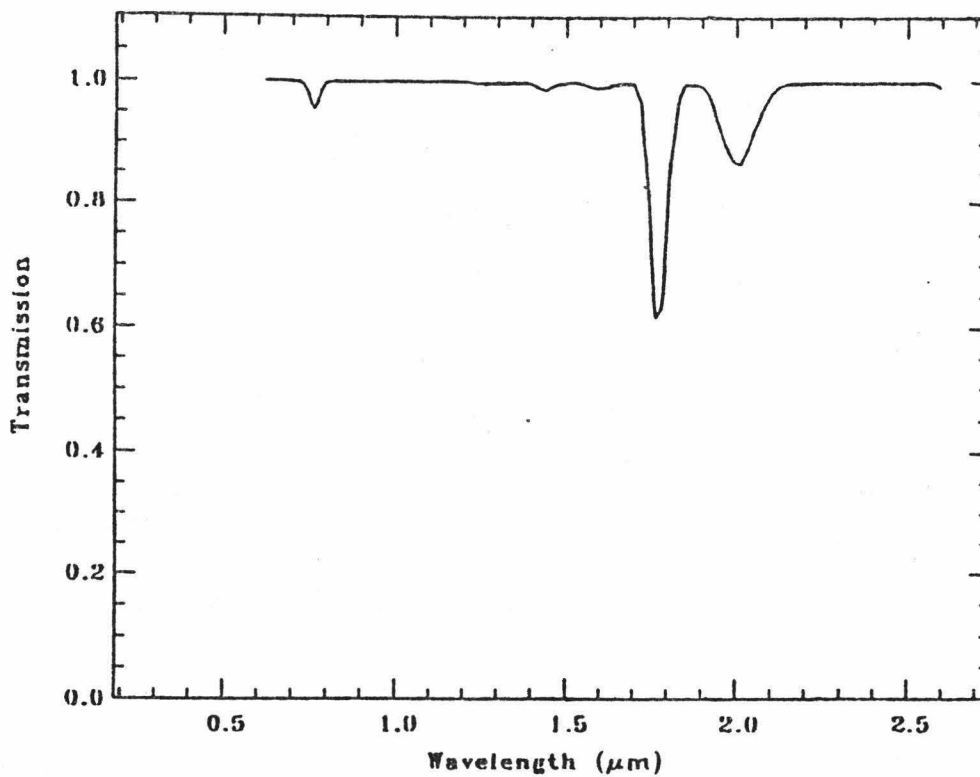
Atmospheric Water Vapor Density

Figure 2.4

Carbon Dioxide (and Other Mixed Gases) Transmission

Spectrum Through a 1km Horizontal Path (at CVF spectrophotometer wavelengths)

(Calculated from LOWTRAN, Kneizys et al., 1980)

Although the CO_2 molecule has three normal modes of vibration at $v_1 = 1.361$ cm^{-1} (.7348cm), $v_2 = 673$ cm^{-1} (14.9 μm), and $v_3 = 2.378$ cm^{-1} (.4205cm), only the latter two are active absorbers.

3. Ozone

Ozone (O_3) is the final important atmospheric absorber in the visible and infrared regions of the spectrum (Kondratyev, 1969, pp.132-139). Like CO_2, ozone behaves as a linear molecule, with vibrational transitions being the primary causes of absorption. The absorptions contributing to the spectrum of ozone are tabulated in Table 2.3.

Other molecules also absorb to an extremely minor degree (Kondryatev, 1969, pp.139-141) in the infrared portion of the spectrum. Although these molecules do not absorb in the spectral region considered in this research (i.e. 0.6 to 2.6 μm), for the sake of completeness these minor constituents and their absorption centers are presented in Table 2.4.

C. SCATTERING

There are two principal mechanisms by which light is scattered by the atmosphere: molecular and aerosol. Both are the result of inhomogeneities in the atmosphere. The first of these is the result of fluctuations in air density which are of the same order of size as molecules; hence the term "molecular" scattering. It is characteristic of this type of scattering that the dimensions of the scattering inhomogeneities are small with respect to the wavelength of the light.

Table 2.3

Ozone Absorption Bands

in the Ultra-Violet and Visible Spectral Regions

Spectral Region (Å)	Name	Notes
2200–3200	Hartley	strong
3000–3450	Huggins	moderate
4400–7500	Chappuis	weak
1050–1750	Schumann–Runge	strong (far UV)
2026–2420	Herzberg	weak

Source: Kondratyev, 1969, pp. 132–134.

Table 2.4

Other Minor Gaseous Absorbers

in the Near–to Mid– Infrared Spectral Region

Gas	Band Center
	(μm)
NH_3	3.0
	6.1
	10.55
CH_4	3.3
	7.7
C_2H_4	3.3
	5.3
	6.9
	10.5
C_2N_2	4.5
	13.5
HCN	3.0
	7.0
	14.0
NO	5.3
N_2O_4	2.5
	5.7
	13.3
H_2S	2.4
	7.75

Source: Kondratyev, 1969, p.140.

The second type of scattering is termed "aerosol" because the scattering inhomogeneities are macro consituents of the atmosphere, such as water droplets or dust particles (Kondratyev, 1969, pp.169-200).

1. <u>Molecular (Rayleigh) Scattering</u>

The theory of molecular scattering was described initially by Rayleigh (although he erroneously attributed the scattering to macro constituents, rather than density fluctuations) (Kondratyev, 1969, pp.171-172), and is often called "Rayleigh" scattering. According to Hvostikov's treatment of Rayleigh scattering (Kondratyev, 1969, pp.172-180), the volume-scattering coefficient, α, (a function of wavelength, λ, and scattering direction, ϕ) for a single scatterer is given by (Kondratyev, 1969, p.176):

$$\alpha_{\lambda, \phi} = (1 + \cos^2\phi) \; (\pi^2(n^2-1)^2) \; / \; (2N\lambda^4)$$

Here n=index of refraction of the scatterer and N=# of scatterers per unit volume. If this function is plotted with respect to the scattering direction, the result is as shown in Figure 2.5, where the direction of incident light is as indicated. The above equation has the general form (Kondratyev, 1969, p.170):

$$\alpha_{\lambda, \phi} = x_\lambda \gamma(\phi)$$

Here, x_λ is a factor which varies with the optical properties of the medium and $\gamma(\phi)$ is the scattering function.
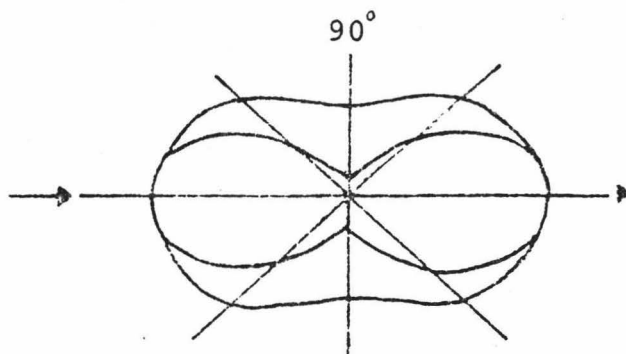
Figure 2.5

Rayleigh Scattering Function

(Adapted from Kondratyev, 1969, p.176)

To obtain the volume-scattering coefficient over the entire volume, this relationship may be integrated over all angles, so that (as derived from Kondratyev,1969, pp.175-177):

$$\alpha_\lambda = 2\pi x_\lambda \int_0^\pi \gamma(\phi)\sin\phi d\phi$$

which becomes:

$$\alpha_\lambda = (2\pi^3(n^2-1)^2) \,/\, (2N\lambda^4)$$

Because $\int_0^\pi (1+\cos^2\phi)\sin\phi d\phi = 8/3$,

then $\alpha_\lambda = (8\pi^3(n^2-1)^2) \,/\, (3N\lambda^4)$.

An important aspect to note about this relationship is that the scattering is proportional to the inverse of the fourth power of the wavelength of the light.

2. Aerosol (Mie) Scattering

The theory of scattering by particles of size equal to or larger than the wavelength of the light is often called "Mie theory" because many of the important mathematical formulae describing this theory were developed by G. Mie (Penndorf, 1962).

- 38 -

The volume-scattering coefficient $f(\rho,\phi,m)$ for large particles (corresponding to $\alpha_{\lambda,\phi}$ given above) is given, for spherical particles, by the Mie formulae (Kondratyev, 1969, p.181):

$$f(\rho,\phi,m) = [(\lambda^2)/(4\pi^2)] \ [(i_1+i_2)/2]$$

$$= \ i(\lambda^2) \ / \ (4\pi^2)$$

Here, $\rho = 2\pi a/\lambda$, a = particle radius, ϕ = scattering angle, m = complex refractive index, i_1 and i_2 = intensities of scattered radiation polarized in two perpendicular planes.

Although this scattering coefficient may be put into the same form as in the Rayleigh case above:

$$\alpha_{\lambda}' = 2\pi\int_0^{\pi}f(\rho,\phi,m)\sin\phi d\phi \ ,$$

the solution is far from simple. Values for $f(\rho,\phi,m)$ have been calculated, however, for the two cases of opaque, totally reflecting particles and for water droplets. The results, for different values of ρ, are given in Figures 2.6a-b. These figures illustrate the "Mie effect", whereby scattering from large particles is predominantly forward-scattering. An important point to note here is that as particle size increases, the wavelength dependence decreases, going to zero at $a=\infty$.
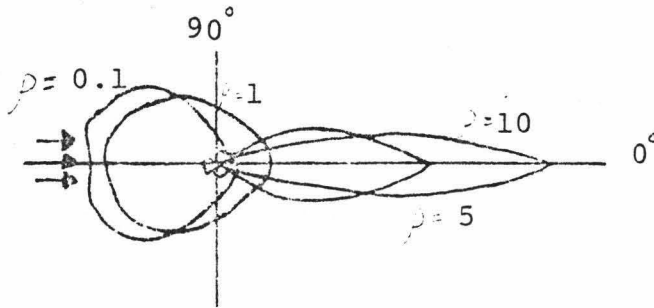
Figure 2.6a

Mie Scattering Function for Opaque Particles

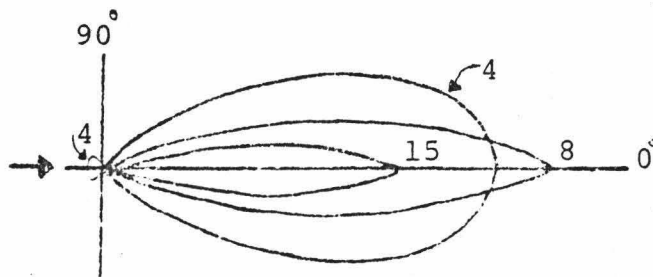(Adapted from Kondratyev, 1969, p.182)

Figure 2.6b

Mie Scattering Function for Water Droplets

(Adapted from Kondratyev, 1969, p.184)

D. MODELLING ABSORPTION AND SCATTERING PROCESSES

Despite the mathematical rigor of the radiative transfer equations, the complexity of atmospheric processes is such that an accurate theoretical model has not been obtained for the earth's atmosphere. Emphasis, instead, has been placed upon obtaining precise numerical, digital computer analyses (Chahine, 1983). While radiative transfer theory is the basis for such models, the models primarily rely upon empirical representations of atmospheric processes; in turn these empirical representations are based upon direct measurements of the atmospheric parameters, both in the field and under simulated conditions in the laboratory (McClatchey et al., 1972).

1. Line-By-Line Models

Empirical atmospheric models may be divided into two basic classes: "Line-by-line" models and "Band" models. The Line-by-line models require precise and detailed understanding of monochromatic spectroscopic line parameters. The average effect of this detailed information then constitutes the spectral information over the spectral interval required (McClatchey et al., 1972). The drawbacks to this technique are first, the fact that actual line parameters are not in all cases known, especially for the upper part of the atmosphere, and second that the computations required are numerically exhaustive, even when performed with a high-speed computer.

2. Band Models

The so-called "Band-model" techniques mitigate both these drawbacks when the accuracy and spectral resolution of a line-by-line analysis is not required. Rather than incorporating actual spectral lines in the model, a band model begins with some assumed configuration of line

- 41 -

parameters (i.e. intensities, half-widths, and line spacings) and adjusts this configuration to accomodate actual band shapes (McClatchey et al., 1972). This configuration may be expressed mathematically as a transmission function of the form:

$$\bar{\tau}_{\Delta v}(v) = f(C(v), \Delta L, P)$$

where P = pressure, ΔL = effective pathlength (equivalent to absorber concentration, and the $C(v)$'s are frequency-dependent absorption coefficients.

Although a number of band models have been developed, the most widely used are the Goody model (1964) and the Elsasser model (1942). Both these models assume a Lorentz shape for the spectral lines; the Elsasser model, however consists of equally-spaced lines of equal intensity, while the Goody model assumes randomly spaced lines having an exponential intensity distribution. The Goody model is most often applied to bands with an irregular line structure (eg. H_2O and O_3); the Elsasser model has been most often applied to bands having more regular structure (eg. CO_2, CO, and O_2) (McClatchey et al., 1972).

The practical application of either of these models involves solving the above transmittance function for the $C(v)$'s for a given species under known (laboratory) conditions and then using the values so obtained to define the transmittance function for different values of P and ΔL, as a function of frequency. The total mean transmittance is obtained as the product of the transmittances of the individual absorber species.

The actual functional forms of the Elsasser and Goody models are the following (McClatchey et al 1972):

Elsasser:

$$\overline{\tau}_{\Delta v}(v) = 1 - \mathrm{erf}[C(v)\ \Delta LP]^{1/2} \ ;$$

where erf = the error function = $\mathrm{erf}(z) = (2/\sqrt{\pi}) \int_z^\infty (e^{-t^2}\ dt)$
and $C(v)$ = an average absorption coefficient.

Goody:

$$\overline{\tau}_{\Delta v}(v) = \exp\{[C'(v)\ \Delta LP]^{1/2}\} \ ;$$

where $C'(v)$ = an average absorption coefficient.

These forms for the atmospheric transmittance function were synthesized into a single expression by King (1959) in the following way:

$$\overline{\tau}_{\Delta v}(v) = f[C'(v)\ \Delta LP^n]$$

The most important aspect of King's generalization is that the variable, n, has been substituted for constants appearing in the previous formulations. The variable, n (which assumes the values of 0 and 1 for, respectively, weak-line and strong-line band approximations), can be varied so that the basic equation above may be applied to a wide range of atmospheric conditions.

E. THE LOWTRAN MODEL

The LOWTRAN model for atmospheric absorptions, which is basically a technique to calculate the transmission and radiance of the atmosphere as a function of wavelength, was developed by McClatchey et al. (1972), and modified extensively by Kneizys et al.(1980). This model follows the form of King's transmittance function. The model actually consists of three transmittance functions empirically determined from laboratory and line-by-line calculations. These three transmittance functions correspond to three different gas species: 1) H_2O (where n=0.9 in King's expression), 2) O_3 (where n=0.4), and 3) the combined contributions of a set of gases (CO_2, N_2O, CH_4, CO, and O_2) assumed to mix uniformly throughout vertical and horizontal extent of the atmosphere (where n=0.75).

The values for n were determined by first taking the logarithm of the inverse of King's equation, which is:

$$n\log P + \log\Delta L = \log f^{-1}[\bar{\tau}_{\Delta v}(v)] - \log C'(v)$$

If, under controlled conditions, the frequency, v, and the average transmittance, τ, are held fixed at various values, then the righthand side of this equation is a constant. In this way, McClatchey et al. (1972) determined that τ could be plotted as a function of $\log \Delta L*P^n$, and so, knowing ΔL and P, n could be determined. Thus, the basis for the LOWTRAN model is that, for a horizontal or constant pressure path, the average transmittance depends upon the product ΔLP^n.

- 44 -

For example, for atmospheric water vapor, this relationship can be expressed as:

$$\Delta L_o (P/P_o)^n = R*w(z)(P/P_o)^{0.9} \; ;$$

where $w(z)$ = water vapor concentration at altitude z (in $gm\text{-}cm^{-2}/km$), and R = range in km. The subscripts denote Standard Temperature and Pressure (STP) quantities.

For a vertical path, this relationship becomes $\int_z^\infty w(z)(P/P_o)^{0.9} dz$.

These expressions are somewhat simplified for the gases (primarily CO_2) assumed to be uniformly mixed within the atmosphere, becoming, for a horizontal path:

$$\Delta L_o = cR(P/P_o)(T/T_o) \; ;$$

where c is the fractional volume concentration of the absorbing gas and R is the range or path length. For a vertical path, this expression becomes:

$$\int_z^\infty (P/P_o)^{0.75}(T_o/T) dz.$$

The results from the LOWTRAN model have been compared to actual atmospheric measurements; the agreement is quite close, within 10% over most of the wavelength range of interest. Two examples of LOWTRAN-produced spectra as compared to measured spectra over this range are shown in Figures 2.7a-b. The chief differences apparent in these comparisons is that some of the fine structure appearing in the

Path Length   27.7 km
Altitude   10,000 ft H_2O in Path   8 - 13 cm
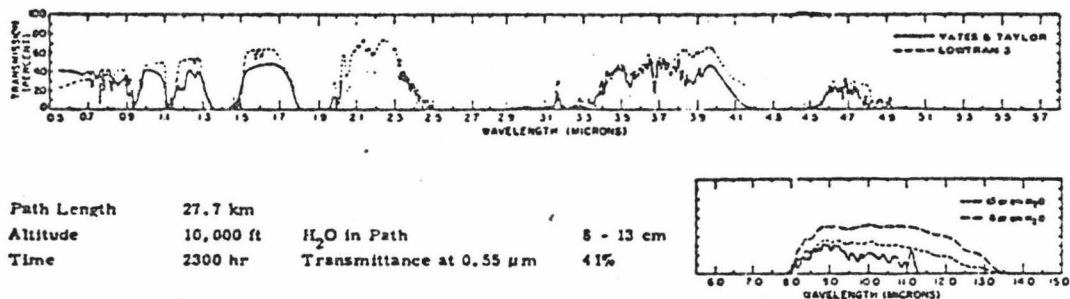Time   2300 hr   Transmittance at 0.55 μm   41%

Figure 2.7a

Comparison of LOWTRAN Predictions With Atmospheric Transmission

Measurements Over 27.7km in the Hawaiian islands, Sept, 1957
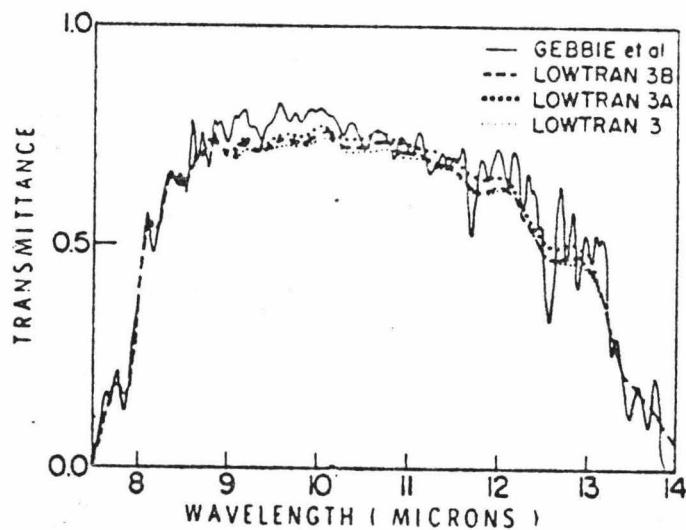
(from Selby and McClatchey, 1975, p.53)

Figure 2.7b

Comparison of LOWTRAN Predictions with Measurements

of Gebbie et al. Over a 1km Nautical Path

(from Selby et al., 1976, p.21)

- 46 -

measurements does not appear in the LOWTRAN data. This is largely the result of the $20cm^{-1}$ resolution of the LOWTRAN spectra. These differences are not a difficulty for the present application in that the LOWTRAN spectra are further degraded by a factor of about 10 in order to make direct comparisons between these data and the measured near--infrared spectra used in the present study. Thus, LOWTRAN data are of more than high enough resolution to resolve the spectral features of interest in solid surface remote sensing.

These LOWTRAN-produced synthetic atmospheric absorption spectra were used, in this research, as the basis for determining the degree of atmospheric absorption affecting remotely-obtained near-infrared reflectance measurements. This comparison was effected by varying within LOWTRAN the values for the water-vapor density given for the bottom three layers (i.e. the lower 3km of the atmosphere) of one of LOWTRAN's atmospheric models. An example showing the results, in the synthetic transmission spectra, of altering this parameter is presented in Figure 2.8. The calibration scheme for which the LOWTRAN synthetic spectra are an integral element is discussed in chapter 3.
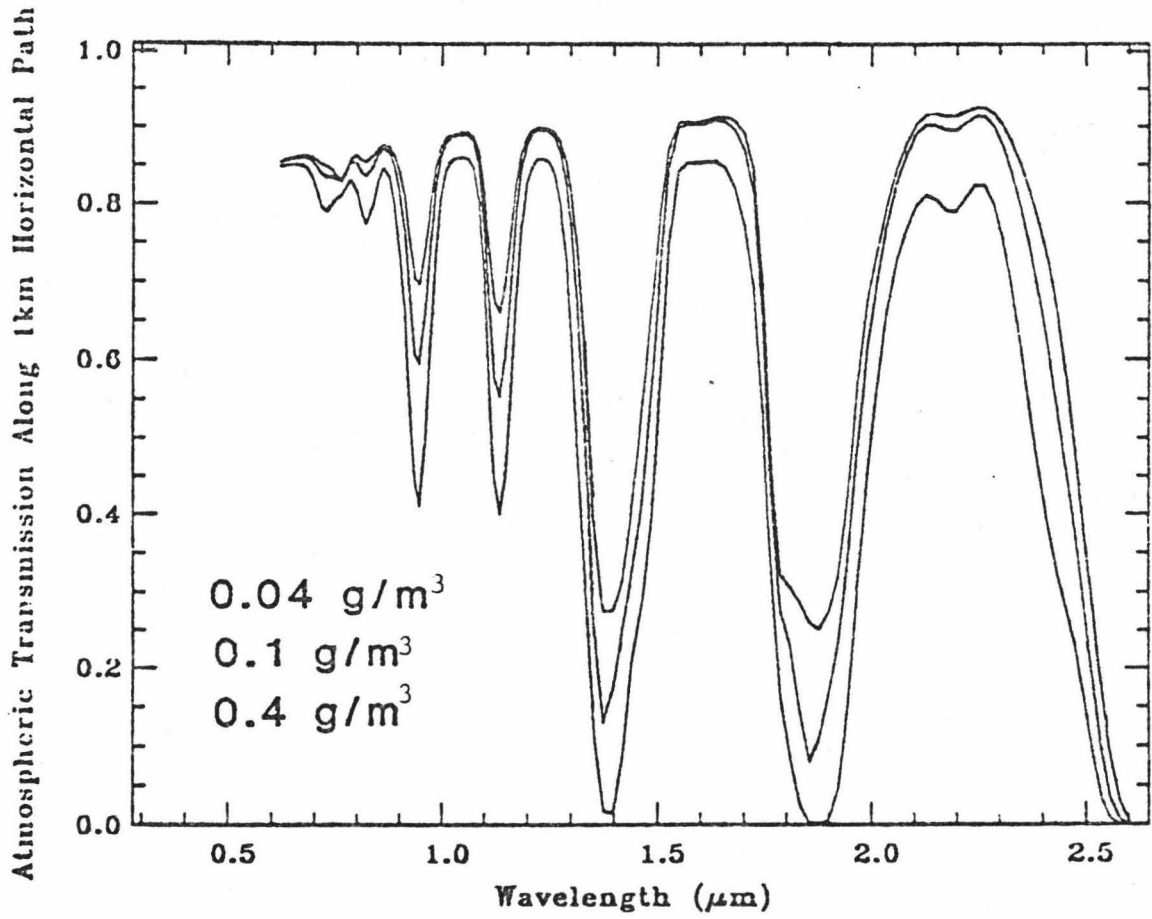
Figure 2.8

LOWTRAN-Produced Atmospheric Transmission Spectra at Various

Atmospheric Water Densities

F. REFERENCES

Chahine, M.T., D.J. McCleese, P.W. Rosenkranz and D.H. Staelin (1983), "Interaction Mechanisms Withn the Atmosphere", in Colwell, R.N., ed., Manual of Remote Sensing, Vol.1: Theory, Instruments and Techniques, American Soc. of Photogrammetry, Falls Church, Virginia.

Elsasser, W.M. (1942), Heat Transfer by Infrared Radiation in the Atmosphere, Harvard Univ. Press, Cambridge, Mass.

Goody, R.M. (1964), Atmospheric Radiation I: Theoretical Basis. Oxford univ. Press, London.

King, J.I.F. (1959), Proc. of the IRIS, 4 (1):164.

Kneizys, F.X., E.P. Shettle, W.O. Gallery, J.H. Chetwynd, Jr, L.W. Abreu, J.E.A. Selby, R.W. Fenn, and R.A. McClatchey (1980), Atmospheric Transmittance/Radiance: Computer Code LOWTRAN 5, AFCRL Environmental Research paper, No.697, AFCRL-80-0067.

Kondratyev, K.Y. (1969), Radiation in the Atmosphere. International Geophysics Series Vol. 12, Academic Press, New York.

McClatchey, R.A., R.W. Fenn, J.E.A. Selby, F.E. Volz and J.S. Garing (1972), Optical Properties of the Atmosphere (3rd ed). AFCRL Environmental Research Paper, No.411, AFCRL-72-0497.

Penndorf, R.B. (1962), "Bibliography on Numerical Computations of Scattering and Absorption of Electromagnetic Radiation for Spherical Particles Based on Mie Theory", Avco Corp., Wilmington, Mass.

Selby, J.E.A. and McClatchey, R.A. (1975), _Atmospheric_
   Transmittance From 0.25 to 28.5 Microns: Computer Code LOWTRAN 3,
   AFCRL Environmental Research Paper, No.513, AFCRL-TR-75-0255.

Selby, J.E.A., E.P. Shettle, and McClatchey, R.A. (1976), _Atmospheric_
   Transmittance From 0.25 to 28.5 μm: Supplement LOWTRAN 3B, AFCRL
   Environmental Research Paper, No.587, AFCRL-TR-76-0258.

CHAPTER III

PROCEDURE AND RESULTS

A. INTRODUCTION

The premise which is the foundation of the technique developed in this research is that the raw near-infrared spectral data can be used as the basic atmospheric "sounding" mechanism to determine the extent to which atmospheric absorption has affected the data set. Hypothetically, this determination can be made through comparison with a set of synthetic spectra generated by a numerical atmospheric model, LOWTRAN, discussed earlier. Before such a comparison is possible, however, the raw spectral data and the synthetic spectra must be put into a similar form. The primary difference between the two data sets is that the LOWTRAN spectra represent percent transmissions of electromagnetic radiation through the atmosphere, with, effectively, no introduction of a detector system into the data. Spectral data gathered by any instrument, however, will necessarily include the response of that instrument. In addition, the synthetic spectral data assumes a source of illumination whose intensity is independent of wavelength, whereas actual spectral data also inherently includes the spectral shape and features of some light source. This light source is the Sun in the case of the field observations employed in this study.

Thus, there are two initial calibrations which must be performed on the raw spectral data before they can be compared to the synthetic transmission data: First, the effect of the solar spectrum must be accounted for, and, second, the response of the detector system must be removed. Additionally, of course, the raw data also include the

spectral response of the objects being measured. Naturally, it would be tautological to suggest that the object spectral response should be removed before the raw data are calibrated, but it has been found in this research that at least the general effect of the object's response may be approximated by defining a continuum for the data and dividing out that continuum. If a similarly defined continuum is also removed from the synthetic spectra, then in theory the two data sets should become fully comparable and the synthetic atmospheric transmission spectrum (representing the atmospheric component) can be divided out of the data. This calibration procedure may be summarized by the following relationship (Eqn. 3.1):

$$R_{lab} \propto R_{cal} = S_{fld} / (F_{sol} * S_{sys} * T_{atm})$$

where R_{lab} = the spectral reflectance of an object measured in the laboratory and calibrated to laboratory standards; R_{cal} = the remotely-obtained reflectance of an object calibrated to match laboratory standards; S_{fld} = the uncalibrated remotely-obtained spectral radiance of an object, in units of flux relative to the instrument; F_{sol} = the solar spectrum, in units of relative flux; S_{sys} = the system response curve, in units of flux relative to the system; and T_{atm} = the atmospheric transmission spectrum, in terms of percent transmission.

The various components of the calibration procedure, expressed in Equation 3.1, may be summarized by the following sequence of operations:

1. Obtain remote near-infrared spectrum.

2. Remove spectral characteristics of illumination source.

3. Remove instrumental system's response.

4. Define and remove continuum from observed spectrum to temporarily remove surface spectral properties and bring data into a form directly comparable with synthetic (calculated) atmospheric transmission spectra.

5. Iteratively fit calculated atmospheric transmission spectra to observed spectrum across wavelength region of two unsaturated water-vapor bands.

6. When a good fit is obtained, divide each observed spectrum by the appropriate calculated atmospheric transmission spectrum, across entire near-infrared spectral range.

7. Factor continuum back into observed spectra to re-introduce surface spectral features.

8. Output calibrated spectra.

This procedure, discussed in detail below, is presented in flowchart form in Figure 3.1.
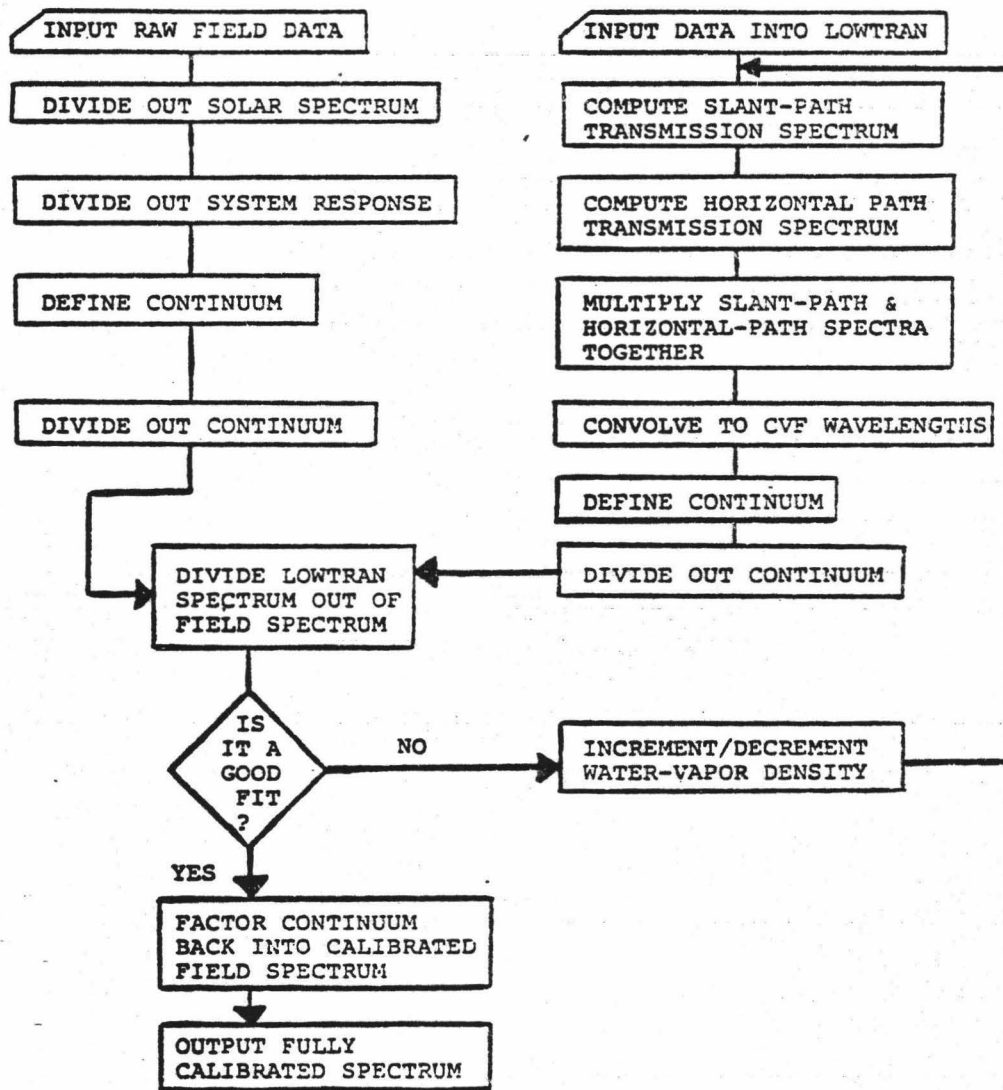
CALIBRATION   PROCEDURE

Figure 3.1

Flowchart for Calibration Procedure

B. COMPONENTS OF DATA AND PRELIMINARY ADJUSTMENTS

1. Field And Laboratory Spectra

The data set used to test this model consists of high resolution ($\Delta\lambda/\lambda=1.5\%$) near-infrared (0.65 μm - 2.55 μm) spectra of several rock samples measured both remotely in the field and in the laboratory using the same indium antimonide (InSb) spectrophotometer. This is a state of the art low-noise infrared instrument (described by McCord et al. 1978, 1980) utilizing a circularly variable filter (CVF). The filter and detector are cooled to liquid nitrogen temperature. The field of view of the instrument can be varied, by varying the aperture used, from 0.013° to 0.067°. In the laboratory this instrument is mounted on a spectrogoniometer; this range in field of view then corresponds to a range of 0.025 cm to 0.125 cm on the object surface. Imaging optics for the field instrument consist of a specially designed 10.8cm diameter, f/10 cassegrain, telescope (focal distance ~36cm) to accomodate what is basically an astronomical instrument designed for a much larger telescope.

The samples measured in the laboratory were measured in the field at a distance of approximately 0.5km. The samples consist of two basalts (a nepheline basalt and an olivine-rich basalt), a carbonate, and a non-geologic white reflectance standard, which was used as a calibration standard in earlier experiments (Singer et al., 1981). The final laboratory-obtained spectra, calibrated relative to the Halon white standard, are shown in Figure 3.2a-d.
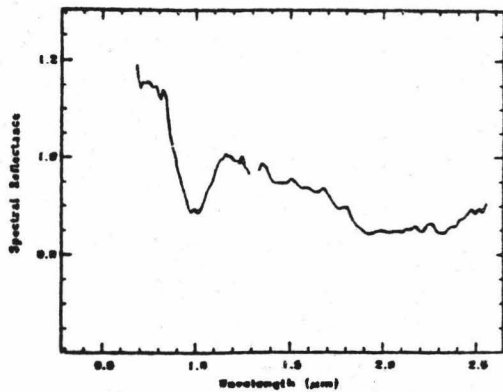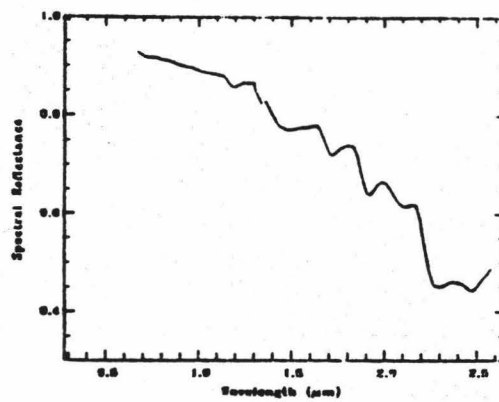
a. Nepheline Basalt
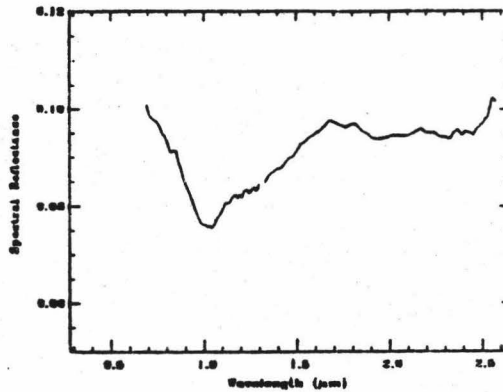
b. Olivine Basalt
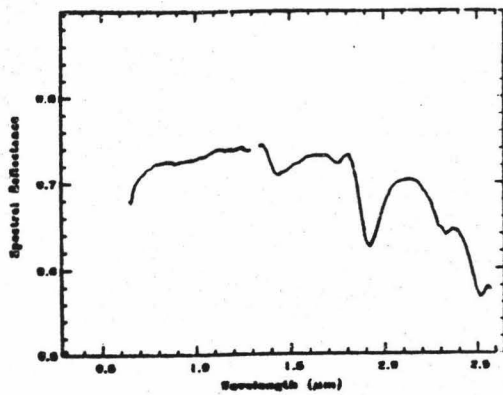
c. Carbonate

d. Field Reflectance
    Standard

Figure 3.2a–d

Laboratory Spectra of Four Samples used for Remote Field Study

The raw data of these samples, obtained in the field, are shown in Figure 3.3a—d. The strong absorption bands centered near 0.935 μm, 1.13 μm, 1.4 μm, 1.9 μm and 2.6 μm correspond to the results of atmospheric absorption (Kondratyev, 1969). As is clear from these samples, the atmospheric absorptions are among the most prominent features of the spectra, tending to be more pronounced than most of the features charactristic of the minerals' reflectance behavior. Since the positions of these atmospheric absorptions are well-known, it is possible to identify in the observed spectra the bands present as a result of atmospheric absorption.

2. Adjustments to Field Spectra

Before the atmospheric absorption bands can be "removed", however, the raw data and the synthetic spectra used to define the atmospheric absorptions must be brought into a comparable form by performing the following calibrations.
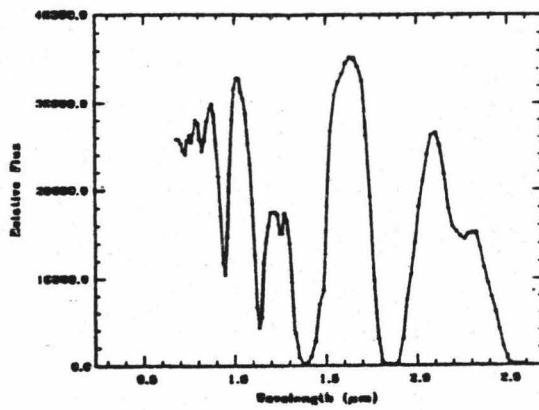
a. The solar spectrum

In order for the field spectra to be comparable to the synthetic spectra, as well as to laboratory-obtained spectra, the inherent effects of the light source—in this case the Sun—must be removed. One generally accepted solar spectrum, used for calibrations of astronomical data, was published by Arveson et al. (1969). This spectrum is shown in Figure 3.4. An alternative to this spectrum was published by Labs and Neckels (1968, 1981) and is shown in Figure 3.5. As it is not clear at this time which of these two spectra is the more accurate (R. Clark, pers. comm. 1983), the more widely used of the two, the Arveson spectrum, was chosen for the present analysis. The difference between these two spectra is everywhere less than 10%, and across most of the spectral
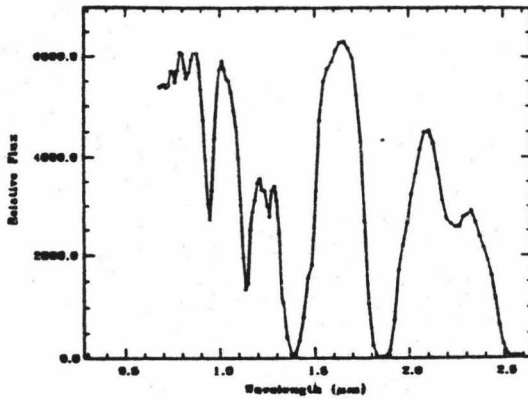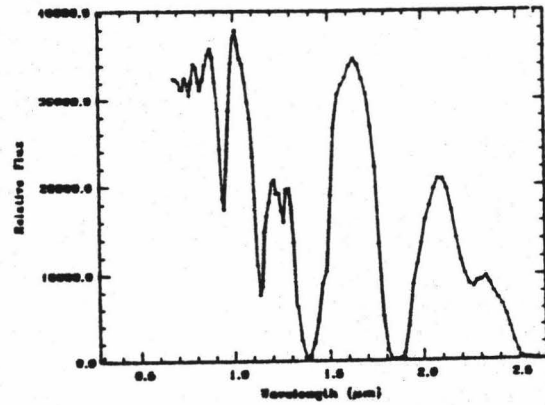
a. Nepheline Basalt
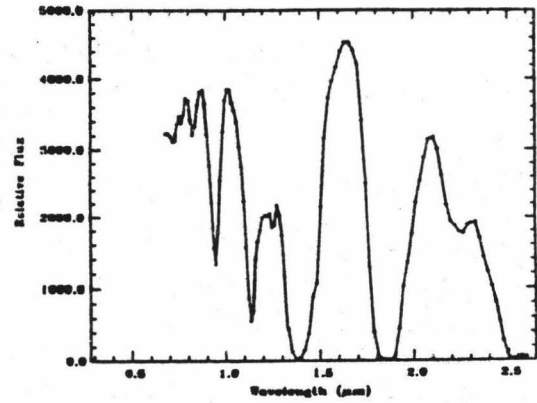
b. Olivine Basalt

c. Carbonate

d. Field Reflectance
Standard

Figure 3.3 a–d

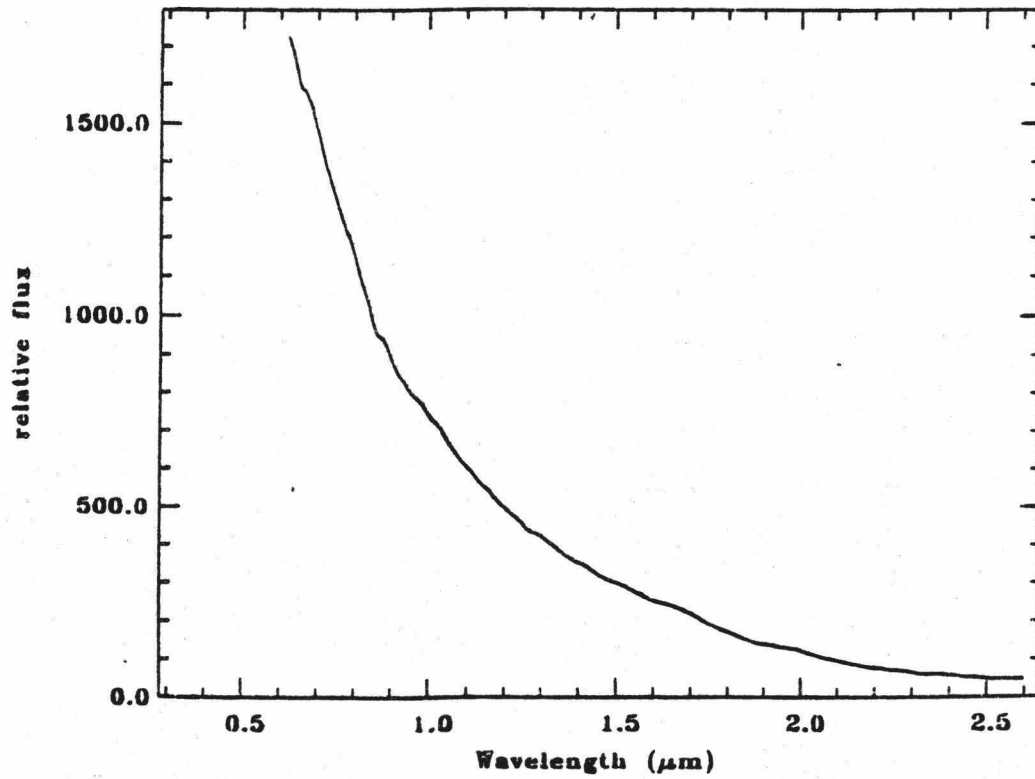**Raw Field Spectra of Four Samples Used in This Study**

Figure 3.4
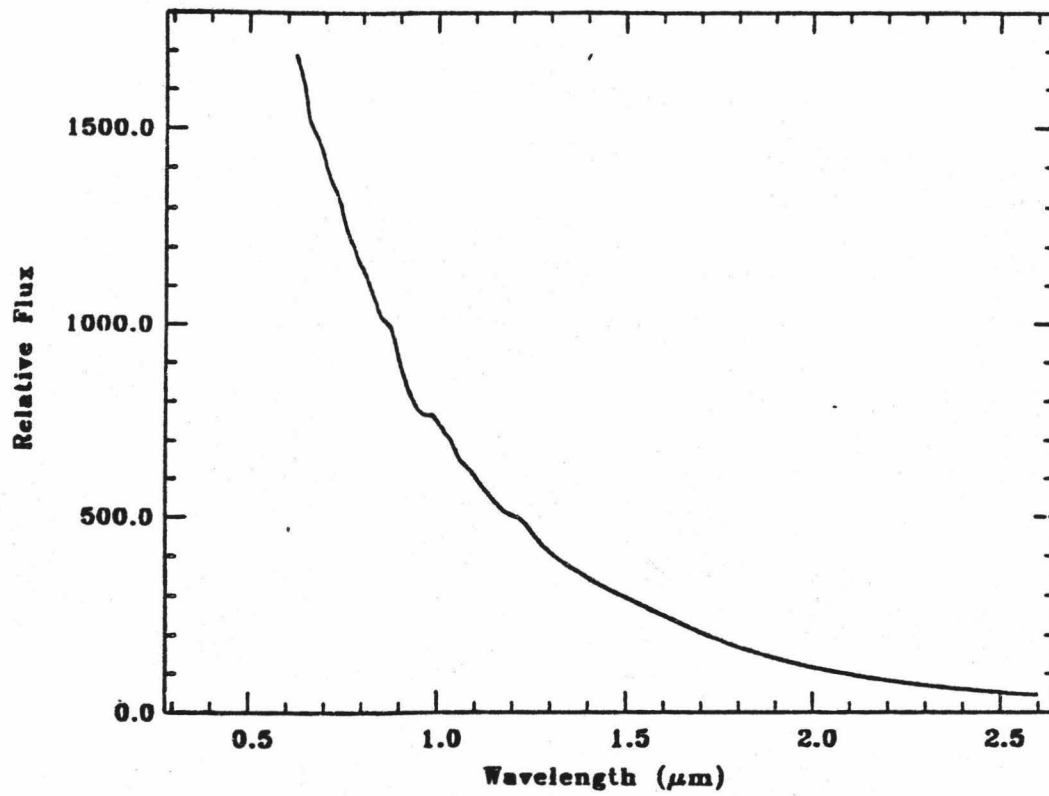
Arveson Solar Spectrum (Arveson et al., 1969)

Figure 3.5

Labs and Neckel Solar Spectrum (Labs and Neckel, 1968, 1981)

region of interest is less than 1%. The raw spectral data, with the solar spectrum divided out, are then used in the following.

b. The system response

The detector and optical system used also introduces into the raw data an undesired wavelength-dependent behavior. This curve is removed in the laboratory automatically when the data are referenced to a concurrently measured white standard. Similarly, the curve is removed from astronomical data when the data are referenced to a standard star set as described in chapter 1). Consequently, prior to the present research, the response curve for the detector system being used was not required and had never been determined; therefore a secondary task of this research was to characterize the system's response curve.

Determining the system's response function requires a light source for which the spectrum is known, against which the measured spectrum is then compared. An approximation to a known source is a laboratory blackbody source which, when calibrated relative to temperature, corresponds very closely to a theoretical blackbody curve at a given temperature. The blackbody emitter used for the present research was a commercially produced device (Infrared Industries, Inc.) obtained through the courtesy of the Hawaii Institute for Astronomy. The particular instrument used is accurate to a temperature of $0.1^{\circ}K$.

The output spectrum from the blackbody source was measured at a temperature of $\sim1173.2^{\circ}K$, near the maximum possible temperature for the blackbody instrument. The spectrometer was employed in a configuration approximating the field setup, but with no telescope. The measured spectra were then divided by a theoretical blackbody curve at the same

temperature. This theoretical curve was calculated from Planck's well-known blackbody equation:

$$E(T) = [(8\pi hc^2)/(\lambda^5)] \; [e^{(hc/\lambda kT)} - 1]^{-1} \; ;$$

where E=energy at wavelength λ (in meters), T=temperature ($^{\circ}$K), c=speed of light (m/sec), h=Planck's constant (=6.6252×10^{-34} Joule-sec), and k=Boltzmann's constant (=1.3806×10^{-23} Joule/$^{\circ}$K).
The curve obtained from this procedure is shown in Figure 3.6. While the upper half (long-wavelength) end of this curve resembled the expected curve, the lower half was clearly not in agreement with expectations. This inaccuracy was the result of the detector becoming saturated at the high flux rate of the long-wavelength end of the filter, with a sufficiently long lag-time that it remained saturated well into the lower end of the CVF.

Fortunately, somewhat comparable data had been obtained previously for this system (P. Owensby, unpub. data, 1981). Although this data was not measured under the exact configuration used with the blackbody setup (a tungsten light was used as the light source and several more mirrors were included along the pathlength), the resulting curve is in good agreement, at the long-wavelength end, with the blackbody measurements of the present author. Since these earlier results did not, however, include the saturation effect at the low-wavelength end of the CVF, these data were employed to represent the system response curve in that region.

Following the generation of synthetic spectra corresponding to the atmospheric absorptions for the four objects being tested, the relationship presented as equation 3.1 was applied recursively to test and
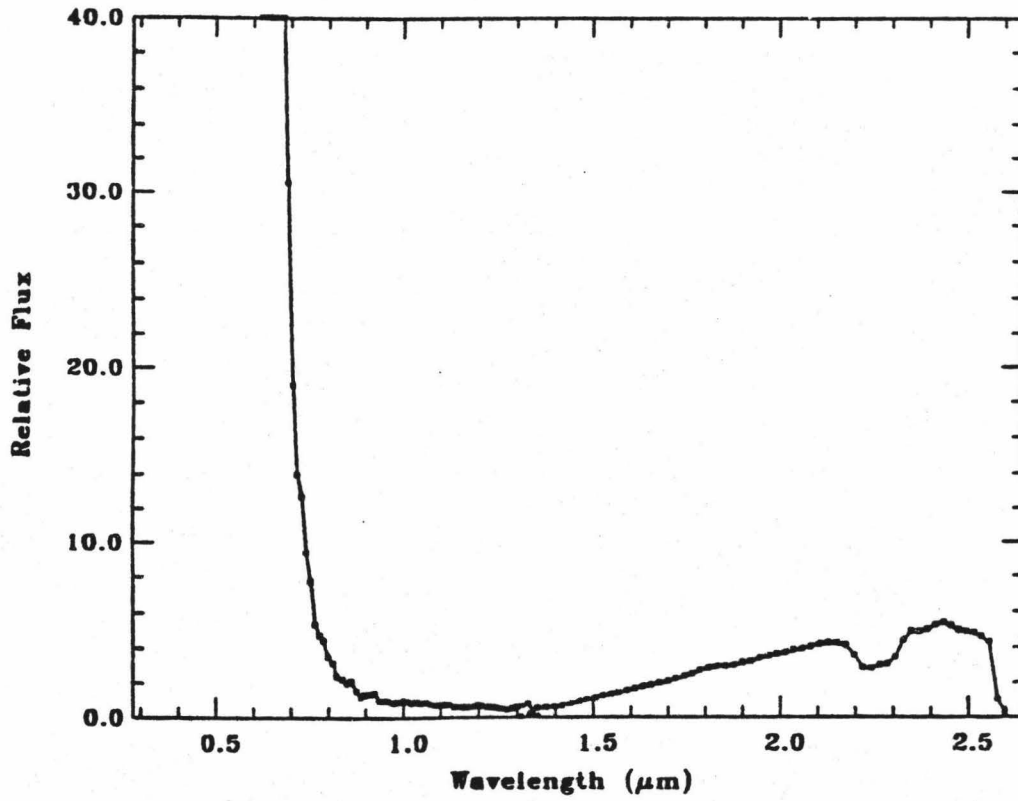
Figure 3.6

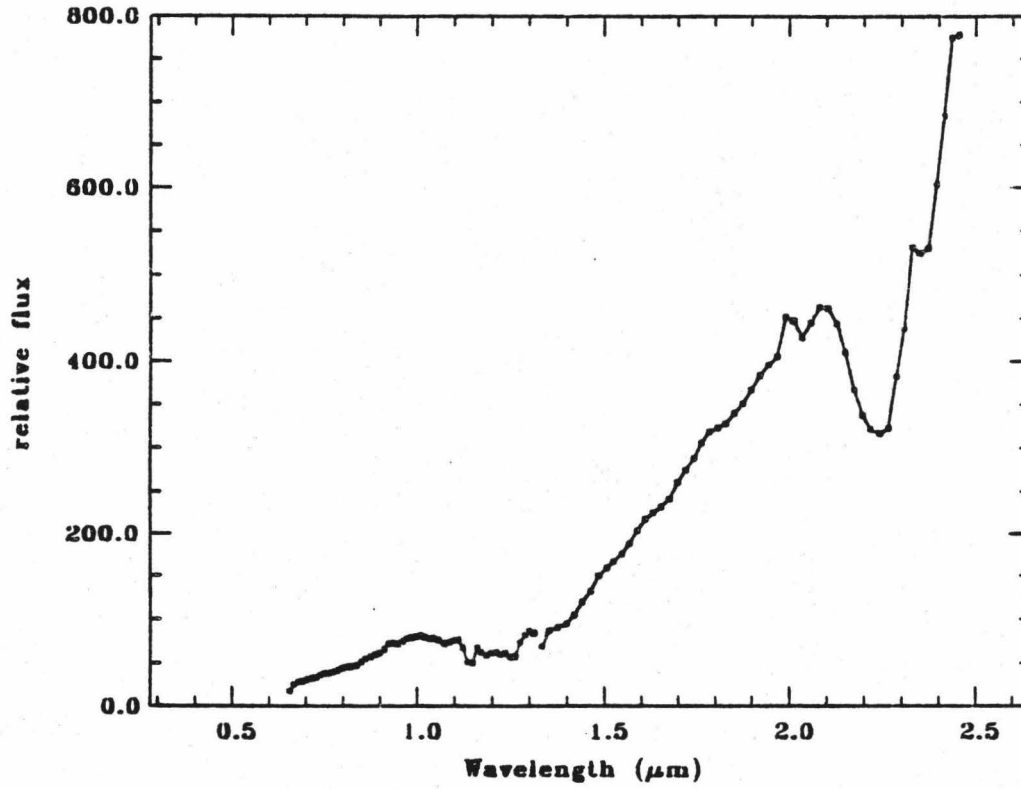System's Response Curve (Showing Saturated Low-Wavelength End)

Figure 3.7

**System's Response Curve Used in This Study**

refine the system's response curve generated by the above methods. This final system's response curve, in units of relative flux, is shown in Figure 3.7.

An additional correction which had to be made to the raw data was a correction to account for the shift in the calibration of the wavelengths as recorded by the infrared system relative to the actual position of the CVF. Although it was known that this calibration had shifted, it was not known to what degree; accordingly, since the LOWTRAN synthetic spectra were convolved (see below) to the actual wavelengths of the filter, the raw data, including the measured system's response curve, were brought into agreement with the wavelength positions of the synthetic spectra. This was done by comparing the shapes and positions of the atmospheric absorption bands in the synthetic spectra with those in the raw data and then the raw data were then shifted to match these positions using a linear interpolation scheme developed by Clark et al. (1982).

Figure 3.8a-d shows the raw data for the four objects with both the system response curve and the solar spectrum divided out. These data have been shifted to account for the wavelength offset.

c. Continuum definition and removal

Removal of a continuum was the final operation performed on the field data in order to bring these data into a mode comparable with the synthetic spectra. The rationale for this continuum removal is twofold: First, if a similarly-defined continuum is also divided out of the synthetic spectra, this brings both data sets into a data range varying from zero to one. Secondly, it was found as part of this research that a continuum, defined as described below, contains spectral information

- 65 -
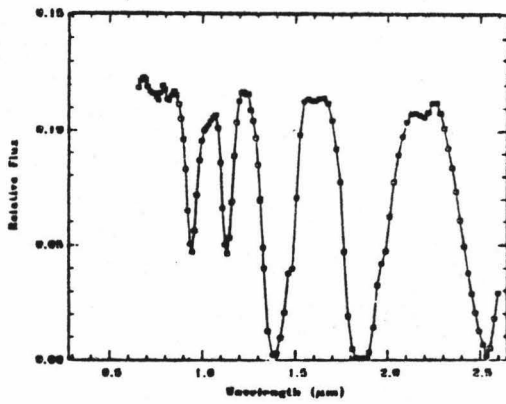
a. Nepheline Basalt
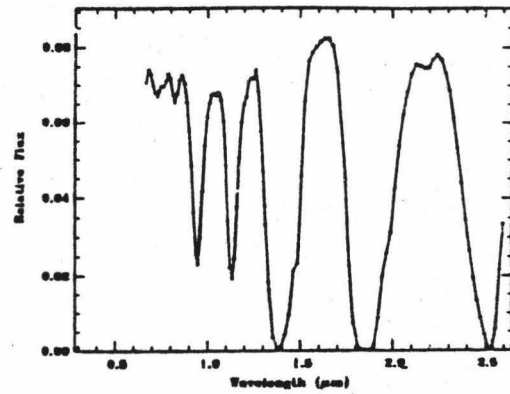
b. Olivine Basalt
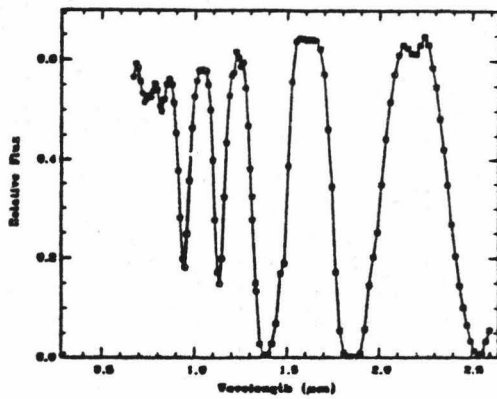
c. Carbonate

d. Field Reflectance
    Standard

Figure 3.8a-d

Field Spectra With Solar and System's Response Removed

about the object surface. While this spectral information is essential and is, in fact, factored back into the object spectra at a later point in the calibration procedure, its temporary removal serves serves to segregate further the atmospheric absorption bands present in the object spectra.

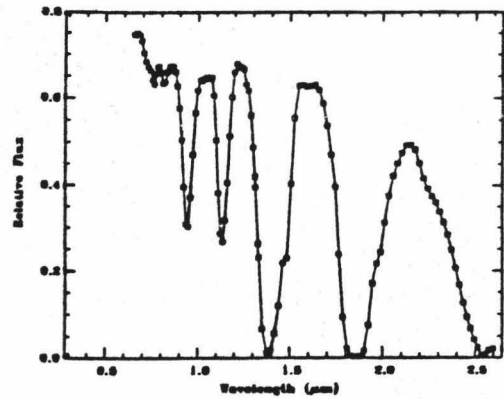The continuum for a given spectrum is defined with reference to the relative reflectance maxima which fall between the atmospheric (principally H_2O) absorption bands. These maxima occur at approximately 0.86μm, 1.05μm, 1.24μm, 1.60μm, and 2.13μm in the calculated atmospheric transmission spectra.

When the solar and system-response spectra are calibrated out of the raw observed data, the atmospheric absorptions dominate the resulting spectra to such an extent that the above intensity maxima also correspond roughly to maxima in the observed data. The points in a spectrum which correspond to the wavelengths above are connected by linear splines and the curve so generated is used as an initial continuum. If this initial curve intersects the data spectrum at any other point(s), then an iterative search is performed, as part of the computer software, to find other local maxima in the data and these points also become part of the continuum; this search is repeated until no further such points exist. The end segments of the continuum, for which there are no maxima to use as a guide, are defined as an extension of the nearest line segment.

Cubic spline continua were initially fit to the data, but the resulting curves were not only very ill-defined at the end-points of the spectrum, but also exhibited the "ringing" behavior often associated with this type of curve-fitting algorithm for even slight differences in point spacing from spectrum to spectrum. In contrast, it was found that

- 67 -

continua defined using straight-line segments not only generated suffi-
ciently smooth, stable curves, but also resulted in decreased computa-
tion time.

Continuua were defined using this straight-line approach for the
four object spectra (with the solar and system-response spectra
removed). These continua are shown in Figure 3.9a-d along with their
respective object spectra. The object spectra with the continua divided
out are shown in Figure 3.10a-d. It is these spectra to which synthetic
atmospheric absorption spectra are compared.

3. Synthetic Atmospheric Transmission Spectra

The LOWTRAN model used to generate the synthetic atmospheric
transmission spectra was described in chapter 2. The particular appli-
cation of that model to the proposed calibration method is described
here.

Included in the LOWTRAN model are data for six standard atmospheric
configurations. The difference between these configurations is in the
profiles (as a function of altitude) for temperature, pressure, water-
vapor density, and ozone density. Five of these six cases correspond to
atmospheric models for different latitude and seasonal regions: tropi-
cal, mid-latitude summer, mid-latitude winter, sub-arctic summer, and
sub-arctic winter. A sixth model corresponds to the 1962 U.S. standard
model atmosphere (Valley, 1965). Additionally, LOWTRAN contains the
option of including the effects of aerosol scattering in the transmis-
sion spectra, for four different aerosol configurations: urban, rural,
maritime, and tropospheric (the tropospheric model is inherent in the
other three as well). These different aerosol models were developed by
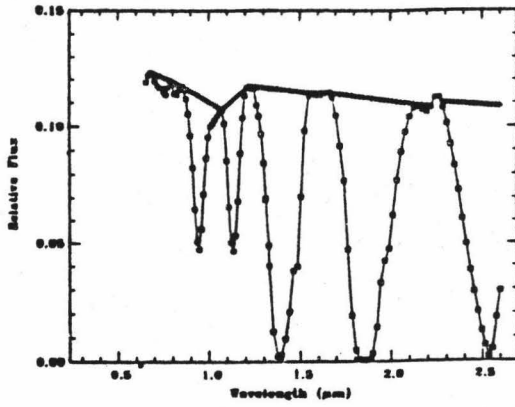
a. Nepheline Basalt   b. Olivine Basalt
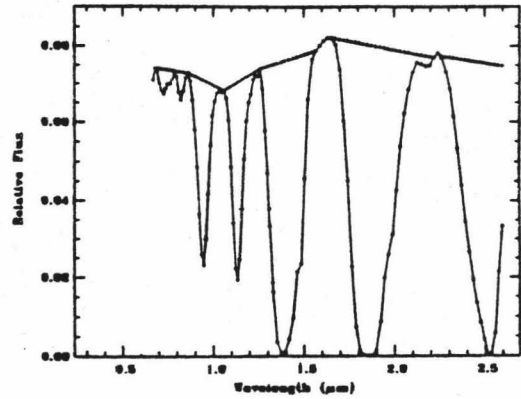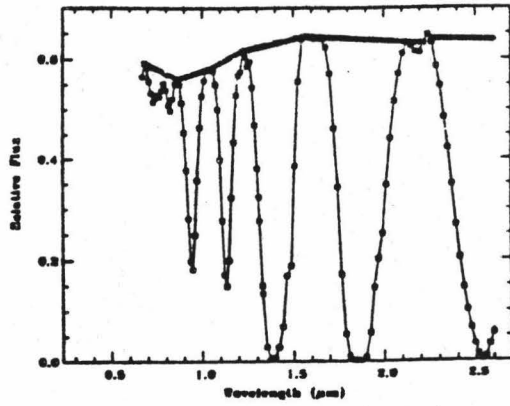
c. Carbonate   d. Field Reflectance
                  Standard

Figure 3.9a-d

Field Spectra With Continua Overlaid

a. Nepheline Basalt

b. Olivine Basalt

c. Carbonate
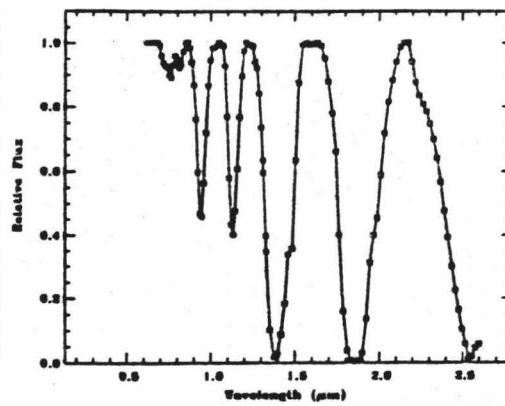
d. Field Reflectance
   Standard

Figure 3.10a-d

Field Spectra With Continua Removed

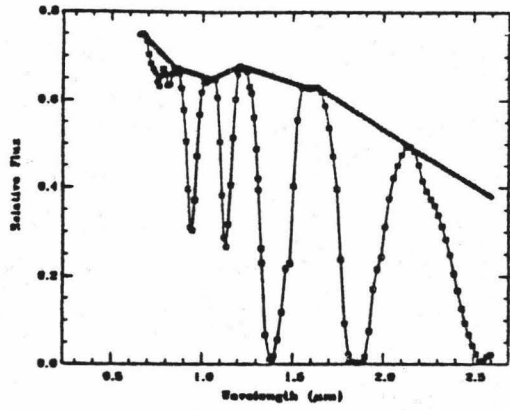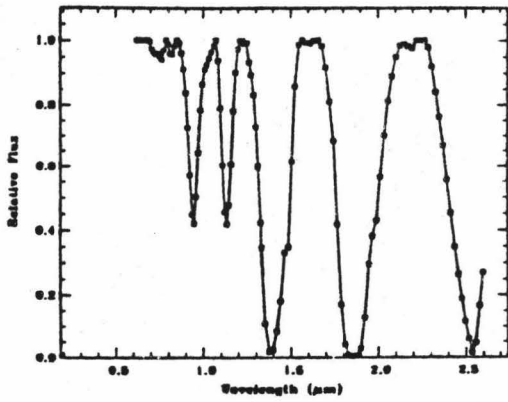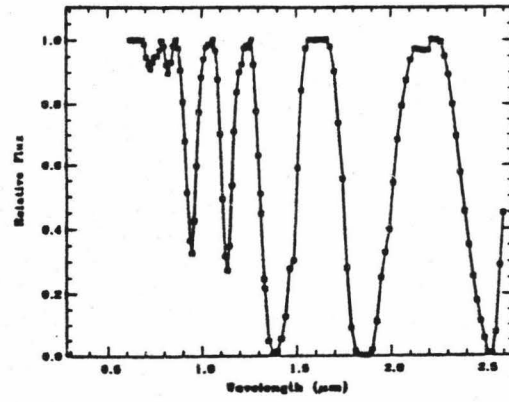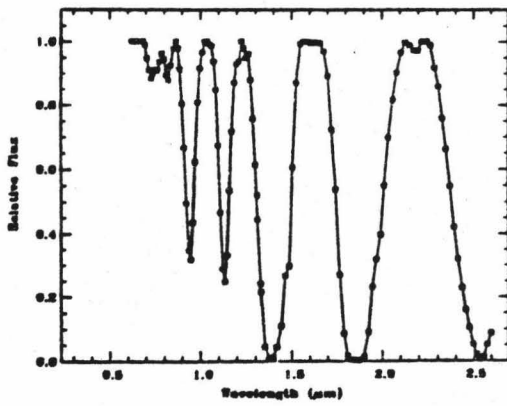Kneizys et al. (1980) and correspond to different species and concentrations of species. For the present data, obtained on Oahu, the tropical profile model and the maritime aerosol model were chosen as most likely to be representative. (LOWTRAN also allows the option of including the effects of volcanic aerosols, as well as the effect of moderate fog (Kneizys et al., 1980), but these options were not explored as part of this work.)

A further aspect of the measuring technique also has to be considered. For this field observation geometry, two paths were followed through the atmosphere: a slant-path from the sun onto the object, and a roughly horizontal path from the object to the sensor. Accordingly, the synthetic spectra obtained with LOWTRAN are the product of a slant-path from roughly sea-level to space and a horizontal path at sea-level. Because the data being analyzed were obtained at mid-morning, the zenith angle of the sun included in this analysis was taken to be 45°.

4. Adjustments to Synthetic Atmospheric Transmission Spectra

a. Convolution

LOWTRAN calculations were performed at a resolution of 10 cm^{-1} over the wavelength range 0.56 μm to 2.8 μm (or 18000.0 cm^{-1} to 3571.0 cm^{-1}). In order for these data to correspond to the field spectra, the synthetic spectra were convolved to correspond to the same resolution and wavelengths as the object spectra. For this convolution, the 120 spectrometer bandpasses (channels) of the Planetary Geosciences Division near-infrared circularly variable filter (CVF) instrument were taken to be Gaussian around their centers, with a height of 1.0 and varying band widths. The centers and widths of these Gaussian bandpasses were

computed by R. Clark and A. Stoltz (unpublished data, 1983). These data were then used in a numerical integration routine to compute the intensities that the synthetic spectra would have at the spectrometer wavelengths. The system's sensitivity response was not included as part of this convolution, but divided out separately as discussed in the section above on the system response curve.

An example of a LOWTRAN synthetic spectrum across the wavelength range of interest, before being convolved to spectrometer bandpasses, is shown in Fiuure 3.11. The same spectrum, except convolved to spectrometer bandpasses, is shown in Figure 3.12. All further LOWTRAN-produced spectra presented below have been so convolved.

b. Continuum definition and removal

Continua were calculated for the LOWTRAN-produced synthetic atmospheric transmission spectra using the same procedure as described in detail above for the observed object spectra; the continua so defined were divided out of the atmospheric transmission spectra. In the case discussed above for the observed spectra, it was found that the continua for those spectra contained information pertinent to the spectral properties of the object's surface. Similarly, although the continua defined for the calculated atmospheric spectra were removed for purposes of comparison between calculated and object spectra, it was also found that these continua closely resembled the spectra resulting from aerosol scattering in the atmosphere (as modelled by LOWTRAN). Thus, the continua defined for the synthetic tramnission spectra were factored back into these data, prior to dividing the synthetic spectra out of the object spectra, as an approximation to removing from the field data the effects of aerosol scattering by the atmosphere.
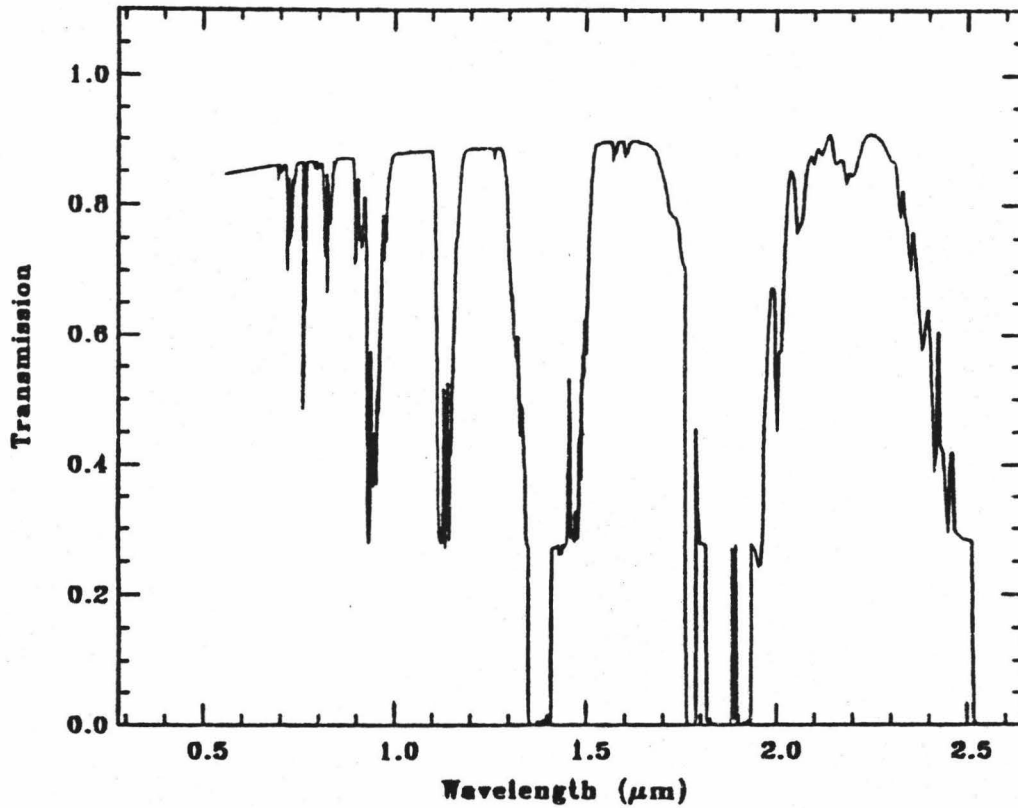
Figure 3.11
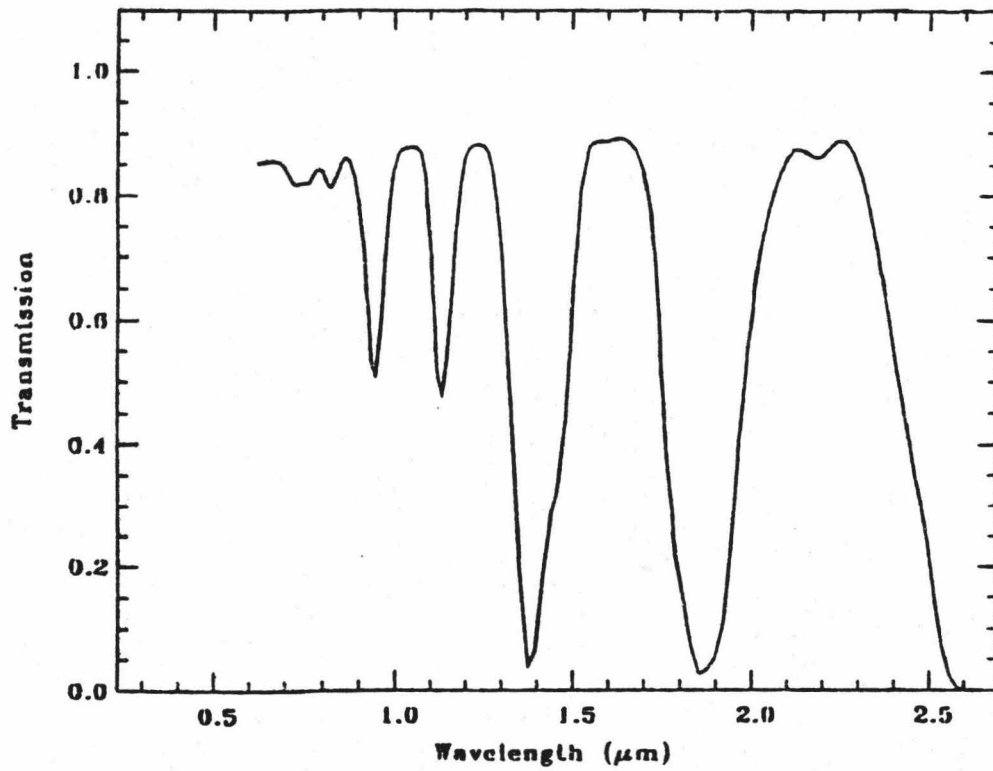
Unconvolved LOWTRAN Atmospheric Transmission Spectrum

Figure 3.12

LOWTRAN Spectrum Convolved To CVF Wavelengths

C. CALIBRATION PROCEDURE

As stated earlier, the hypothesis underlying this calibration technique was that the raw near-infrared spectral data, themselves, contain sufficient information to establish the contribution of the intervening atmosphere to these same near-infrared spectra. Further, it was assumed that an existing atmospheric model, LOWTRAN, could be used to extrapolate across the whole wavelength region of interest the atmospheric information contained in the near-infrared spectra. The technique developed based upon these hyptheses has a two-fold objective: 1) To obtain, through LOWTRAN, the appropriate atmospheric transmission spectra; and 2) To use these calculated spectra to remove the atmospheric components from the object spectra, i.e., to calibrate the object spectra. In order to accomplish these two objectives, criteria for identifying the "appropriate" transmission spectra must first be established, and then a method determined for applying these criteria.

1. Definition of Appropriate Transmission Spectra

Simplistically, what is required are the transmission spectra which, when divided out of the object spectra, will best remove the atmospheric components from those object spectra and in doing so yield the desired, calibrated spectra; these spectra would then be in a form comparable to laboratory-calibrated spectra obtained of the same objects. The practical implementation of this definition required identifying certain limited criteria for the "best-fit" transmission spectra. Because atmospheric water vapor is by far the most significant contributor to the atmospheric spectrum, the portion of the spectrum encompassing two of the unsaturated water-vapor absorption bands of intermediate depth was used as the region to test for goodness-of-fit. The procedure used to calibrate the object spectra was based upon the

assumption that by varying the water content of the model atmosphere in a systematic way, the best-fit atmospheric transmission spectra could then be determined.

As the amount of water vapor in the atmosphere varies, both the shape and depth of the H_2O absorption bands vary as well. At first the change in band depth is nearly linear, becoming more asymptotic as the band center saturates and the wings of the band begin to broaden (Goody, 1964). If an atmospheric band is saturated, then this indicates that no information pertaining to the target is reaching the sensor in the wavelength region near the center of that band because the light in that region has been fully absorbed by the atmosphere. The three deepest atmospheric bands, centered near 1.4 μm, 1.9 μm, and 2.6 μm, will, at sea level, reach saturation in virtually all cases. Thus, remotely obtained spectra of objects on or near the earth's surface will always have at least three regions over which effectively no additional spectral information is available. The four smaller atmospheric bands centered near 0.72 μm, 0.81 μm, 0.94 μm and 1.13 μm will not, however, in most cases be fully saturated, and spectral information across these bands and in the regions between the large bands should therefore be recoverable. Accordingly, the wavelength region across two of these smaller spectral bands was used to determine when the synthetic spectra sufficiently matched the object spectra; in particular, the spectral region across the two bands centered near 0.94μm and 1.13μm were used. Because this wavelength region also encompasses bands of geological interest (eg. pyroxene and olivine crystal-field-bands), which are also apparent in the object spectra being analyzed, it was felt this region would be doubly diagnostic as to the effectiveness of the procedure.

2. Measures of Goodness-of-Fit

Four specific measures of goodness-of-fit (with regards to the two bands at 0.94 μm and 1.13 μm) were tested. Two of these were comparative measures between the object spectra and the calculated transmission spectra; the other two were tests performed on the spectra resulting when the calculated transmission spectra (with the appropriate continua removed) were divided out of the object spectra (with the appropriate continua removed). These latter two measures were actually testing the linearity of these "divided" spectra in the test region; the assumption being that, if the continua removed all of the spectral features unique to the object spectra, then dividing out the appropriate atmospheric spectra would yield values for reflectance very near to one. The two measures used to test this assumption were: the coefficient of correlation ("Pearson's R-value") relative to the line of best fit through the data points encompassing the two bands and the average reflectance values of the points across each of the two bands in the test region (values which should be very near to one). The two comparative measures which were applied between the object and calculated spectra were: the depths and positions of the minima for the two bands in the test region and the average depth of the three bottom-most points of the bands (the bands are sharp enough so that these three points are always contiguous).

The most diagnostic of these measures—that is, the measure giving the most useful information as to how to vary the assumed water content of the atmosphere so as to yield the appropriate synthetic spectra—was the average band depths of the three points defining the band minima for the two bands. This value exhibited a predictable relationship with changes in the water-vapor density of the bottom (horizontal) layer of

- 77 -

the atmosphere. The exact point defining the band minimum was identical in all cases for the object and synthetic spectra. The other measures tested varied less predictably than the average band minimum value, and so did not appear to provide any additional, useful, information. In fact, the two parameters measured against the divided spectra seemed to provide a better measure of how fully the continua removed surface spectral features from the object spectra. Accordingly, the average depths of the two water-vapor absorption bands were used as the criteria for determining the goodness-of-fit of the synthetic atmospheric transmission spectra to the object spectra.

3. Iterative Technique

As discussed above, the different synthetic atmospheric transmission spectra were obtained by varying the water-vapor content (in terms of density) of the model atmosphere. Naturally, varying the density, within the LOWTRAN model, of the water vapor in the bottom, horizontal layer of the atmosphere had a greater effect on the resultant transmission spectrum than varying the density in other layers; in fact, varying this parameter alone would have been sufficient to obtain the appropriate synthetic transmission spectra. However, in order to maintain the integrity of the atmospheric water density profile within LOWTRAN, it was actually necessary to vary the water density within the bottom three layers of the model atmosphere. Although the resultant water density profile for each case is probable, no suggestion is made here that the profile so achieved corresponds to the actual structure of the atmosphere at the time the spectral measurements were obtained—it is merely one of many possible models.

The procedure to obtain the best-fit atmospheric transmission spectra was iterative, where the variable used to drive the iterative process was the water-vapor density of the model atmosphere. The following four steps formed the basis for the iteration:

a. Assume some set of initial values for the water-vapor density and calculate atmospheric transmission spectra.

b. Test for goodness-of-fit between object spectra and calculated atmospheric transmission spectra, using the criteria described above.

c. If the goodness-of-fit is sufficient (i.e. if the difference in band depths between object and calculated spectra are below a specified value), divide calculated atmospheric spectra out of object spectra, multiply object continua back in and output calibrated spectra; otherwise go to step 4.

d. If the goodness-of-fit is not good enough, increment or decrement, as appropriate, the assumed water-vapor density, recalculate the synthetic atmospheric transmission spectra, and return to step 2.

D. RESULTS

The foregoing iterative calibration process was applied to the four near-infrared samples discussed earlier. These object spectra (with the solar spectrum, system's response curve, and continua removed) are presented in Figure 3.13a-d along with the appropriate LOWTRAN-computed transmission spectra (with continua removed). The final, calibrated spectra were obtained by dividing these object spectra by these atmospheric spectra and then factoring the object continua back in; these calibrated spectra, along with their respective laboratory counterparts, are shown in Figure 3.14a-d.

1. Comparison With Laboratory-Calibrated Spectra

The ultimate test of how well the synthetic atmospheric transmission spectra represent the atmospheric absorptions affecting the object data is the comparison of the calibrated field data to laboratory-obtained spectra for the same object; these comparisons are presented in Figure 3.17a-d. Before discussing this figure, it is pertinent to consider the ways in which laboratory data intrinsically differs from field data, even when that field data is calibrated to laboratory standards. Barring the atmospheric effects, there are two main differences between laboratory and field data: 1) The size of the sample area which is measured; and 2) The geometry (phase angle, illumination angle, etc.) of the measurement set-up. In many cases the latter of these may be controlled in the laboratory so as to approximate the geometry of the field measurements. In theory, the first of these may also be accounted for in
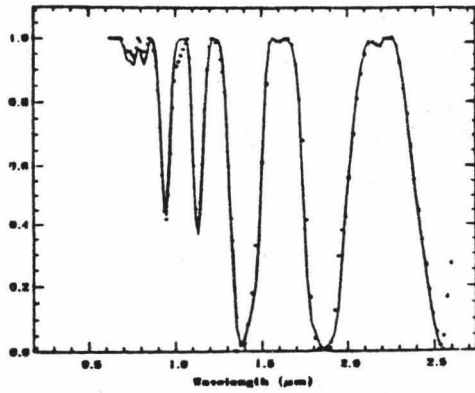
a. Nepheline Basalt
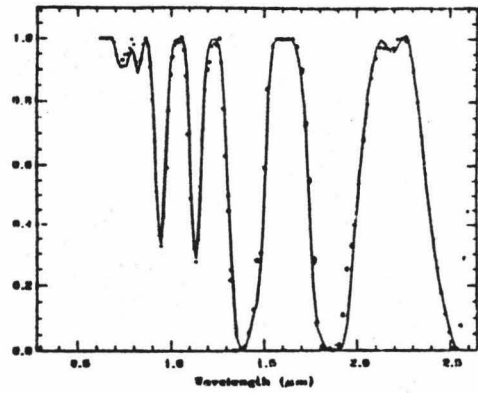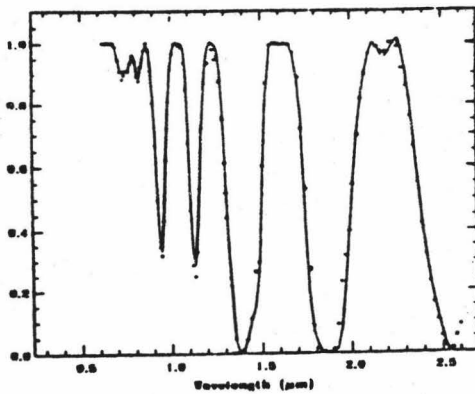
b. Olivine Basalt

c. Carbonate

d. Field Reflectance
    Standard

.... Field Data
_____ LOWTRAN data

Figure 3.13a-d

Four Field Spectra Overlaid With Comparable LOWTRAN Spectra

a. Nepheline Basalt
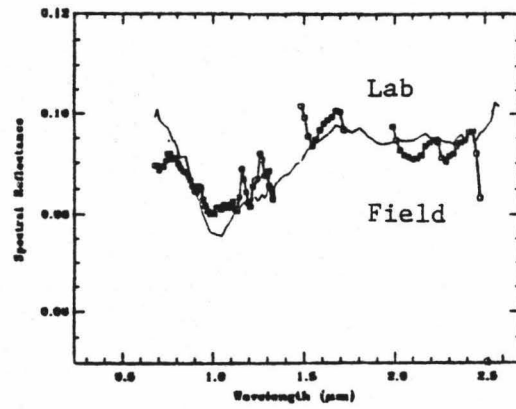
b. Olivine Basalt
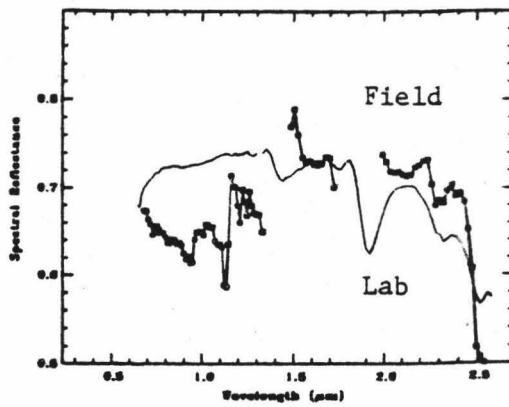
c. Carbonate
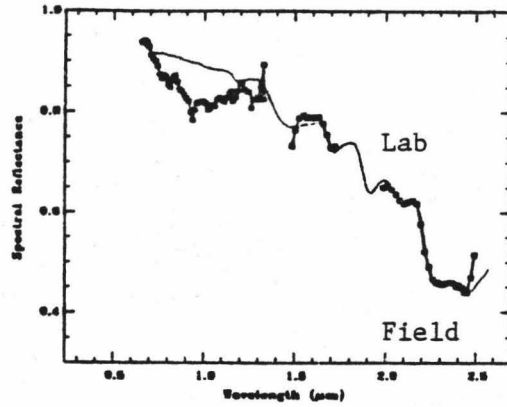
d. Field Reflectance
   Standard

Figure 3.14a-d

Final Calibrated Field Spectra

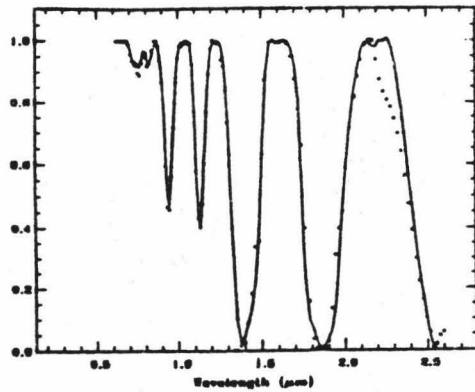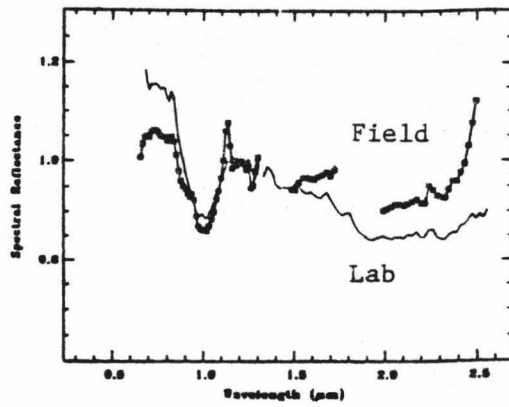the laboratory by obtaining measurements of a number of points on a large enough sample; this is not, however, a very practical approach. Rather, it is generally assumed that a selection of points measured of a sample in the laboratory sufficiently approximates the remotely-acquired field data; this was the approach taken in the present research. The validity of this assumption is dependent upon the selection of sample points and the homogeneity of the sample, as well as the differences in surface scatter geometry in integrating over a large area as compared to several small points.

The samples used in this study were relatively homogenous and care was taken to obtain laboratory measurements of the same exact whole-rock surface as was measured in the field. The laboratory set-up was also arranged to approximate the field geometry. However, these approximations are, after all, only approximations and, undoubtedly, some intrinsic differences were still introduced between the two data sets.

The discussion below outlines the areas where the calibration technique was successful and where the technique was weak or inconsistent. This assessment is made primarily by comparing the calibrated field data to the laboratory data for the same objects, even though these two data sets may not be identical.

2. Strengths of the Calibration Technique

Examination of Figure 3.17a-d yields the following summary of the strengths of this technique:

a. The general shape of the spectra (as apparent in the laboratory spectra) was preserved for the two basalt samples and for the white standard, and somewhat for the long-wavelength region of the carbonate spectrum.

b. The 1-μm crystal field band of olivine was preserved for the olivine-basalt spectrum.

c. The 1-μm crystal field band of pyroxene was preserved for the nepheline basalt sample.

d. The depths of these two band features, although not exact, is very similar for laboratory and field data.

e. Although some absorption features occuring in the long-wavelength end of the spectra are lost because they are coincident with saturated water vapor bands, some absorption features in this region are preserved moderately for the nepheline basalt (these are the broad 2-μm crystal-field band of pyroxene as well as some very minor fluctuations which are probably the result of surface oxidation), and preserved quite well for the white standard. Two of the carbonate absorptions, near 2.3μm and 2.6μm, are also evident.

3. Weaknesses of the Calibration Technique

The following weak points in the calibrations are also evident from Figure 3.17a-d:

a. The most obvious weakness is in the failure of the calibration to preserve the general spectral shape of the carbonate spectrum.

b. An apparently spurious absorption-like feature exists near 1 μm in the field spectra, but not in the laboratory spectra, for the white standard and the carbonate sample.

c. Although the field spectra have been scaled so as to roughly match the laboratory spectra, the 1-μm crystal field bands of olivine and pyroxene appear to be generally weaker in the field spectra.

d. Spectral information is, of course, lost in the regions of the centers of the saturated water-vapor absorption bands, but there is also information lost over most of the width of these bands, rather than just near the centers.

4. Evaluation of the Technique

The above comparisons clearly demonstrate the effectiveness of the calibration technique developed in this research. In all cases, useful mineralogical information contained in the remotely-sensed near-infrared data was successfully extracted from the raw (atmosphere-affected) data and enhanced through the calibration process—without reference to an external standard. The calibrated spectra obtained for three of the samples were quite similar to the laboratory spectra for these objects.

The notable exception to the success of the technique was the calibration for the carbonate sample; although the general shape of the long-wavelength end of this spectrum was moderately well-preserved, the low-wavelength end is quite different between the laboratory and field spectra, exhibiting the spurious absorption-like feature also seen in the spectrum for the reflectance standard. Also, the overall slope across the spectrum is quite different between laboratory and field data. The possible sources of these errors are considered below.

The two greatest unknowns introduced into the calibration process are the scattering properties of the atmosphere and the particulars of the system's response curve, especially in the low-wavelength end of the spectral region. Both of these factors, therefore, represent potential sources of error in the calibration. It seems quite likely that the broad, spurious absorption-like feature appearing in the field spectra for the white standard and the carbonate sample is the result of error in the system's response curve; this is the region of the curve which was estimated from a previous series of measurements. It may also be that the relatively more shallow depth of the 1-μm bands in the basalt field spectra is the result of this estimated response curve. An improved system's response curve is clearly a necessary first step in refining this calibration technique.

It is not clear what is causing the differences in slope between the laboratory and field spectra. Given that the difference is not consistent for all the samples, it may be that its primary cause lies in the differences noted earlier which are intrinsic between laboratory and field data; or variations in atmospheric scatter, which were not explicitly considered as part of this research, may be the source of the observed slope differences.

E. REFERENCES

Arveson, J.C., R.N. Griffin, Jr., and B.D. Pearson, Jr. (1969),
"Determination of Extraterrestrial Solar Spectral Irradiance from a
Research Aircraft", Applied Optics, 8 (11):2215-2232.

Clark, R.N., J.A. Hoover, R.K.L. Kam (1982) "SPECtrum Processing
Routines (program SPECPR), Planetary Geosciences Internal Report,
Hawaii Institute of Geophysics, Univ. of Hawaii, Honolulu.

Goody, R.M. (1964), Atmospheric Radiation I: Theoretical Basis,
Oxford Univ. Press, London.

Infrared Industries, Inc., Blackbody Model # 463, Serial #597D,
Los Angeles, CA.

Kneizys, F.X., E.P. Shettle, W.O. Gallery, J.H. Chetwynd, Jr,
L.W. Abreu, J.E.A. Selby, R.W. Fenn, and R.A. McClatchey (1980),
Atmospheric Transmittance/Radiance: Computer Code LOWTRAN 5, AFCRL
Environmental Research paper, No.697, AFCRL-80-0067.

Kondratyev, K.Y. (1969), Radiation in the Atmosphere, International
Geophysics Series Vol. 12, Academic Press, New York.

Labs, D.T. and J.A. Neckel (1968) Z. Astrophysik, 69 (1):15-22.

Labs, D.T. and J.A. Neckel (1981), Solar Physics, 74: 231-249.

McClatchey, R.A., R.W. Fenn, J.E.A. Selby, F.E. Volz and
J. S. Garing (1972), Optical Properties of the Atmosphere (3rd ed).
AFCRL Environmental Research Paper, No.411, AFCRL-72-0497.

McCord, T.B., R.N. Clark and R.L. Huguenin (1978), "Mars: Near-Infrared
Spectral Reflectance and Compositional Implications." Journal of
Geophysical Research, 83 :5433-5441.

McCord, T.B., R.N. Clark and R.B. Singer (1982), "Mars: Near-Infrared Reflectance Spectra of Surface Regions and Compositional Implications." _Journal of Geophysical Research_, _87_: 3021-3032.

Singer, R.B., P.L. Blake, P.G. Lucey and T.B. McCord (1981), "Application of Reflectance spectroscopy to Geologic Mapping on Earth: Stratigraphic Units in Kilauea Caldera", Annual Progress Report, JPL Contract #955722, Planetary Geosciences unpublished report.

Sissenwine, N., Grantham, D.D. and Salmela, H.A. (1968), "Humidity Up to the Mesopause", AFCRL-68-0550.

Valley, S.L., ed., (1965) Handbook of Geophysics and Space Environments, Air Force Cambridge Research Labs (AFCRL), Office of Aerospace Research, U.S. Air Force, Cambridge, MA.

1.7u 67.9s 2:01 57%

CHAPTER IV
SUMMARY AND FUTURE APPLICATIONS

The results, as discussed in the previous chapter, of the atmospheric calibration process developed in this research, demonstrate the utility of employing this analytical method to calibrate remotely-obtained near-infrared reflectance measurements. There are, however, refinements which could and should be made in the technique; following which the technique should be extended and made applicable to the kind of image data which will be obtained from high-resolution mapping spectrometers such as the Airborne Imaging Spectrometer (AIS). These refinements and embellishments are discussed below.

A. REFINEMENTS IN TECHNIQUE

Most of the refinements and improvements to the calibration technique which are considered here have been identified in the previous chapters. The following discussion serves primarily to summarize.

1. The Instrument Response Curve

A first-order refinement should be to obtain a more precise system's response curve for the infrared CVF instrument. Because of the problem of detector saturation encountered using the high-intensity laboratory blackbody source, the low-wavelength portion of the response curve obtained as part of this research was estimated from previous measurements (P. Owensby, unpub.data, 1981). There are two approaches which would avoid this problem: Either a low-intensity light source of known spectral characteristics might be obtained, or the same blackbody

source could be employed, but with the CVF held fixed at each of the low-wavelength positions on the filter. The response curve so obtained would be in units of relative flux, because the relationship between data counts which the detector records and absolute flux units is not known. It would be very desireable to calibrate the detector counts to absolute units, as this would then allow for the system response curve to be obtained in absolute units and, hence, for remotely-obtained data to be calibrated to absolute reflectance.

Although the instrument system response is often included as part of the instrument bandpasses, in many other instruments an accurate system response curve is necessary if this calibration technique is to be applied to data obtained from systems other than the Planetary Geosciences near-infrared instrument. If this system response function is unknown or poorly known, it is evident from the present research that an estimate of the response may be obtained, provided that field data exist for a laboratory-calibrated object. The present calibration scheme might then be recursively applied, using the relationship expressed in Eqn. 3.1, to obtain the estimated response curve. Such a recursive formulation would begin with an approximate response curve, and then, through several backward iterations of the calibration technique, obtain improvements upon this initial estimated curve. Of course, the curve obtained using such a procedure would be in units of relative flux.

2. The Iterative Procedure

Certain of the weaknesses in the calibrations noted in the previous chapter might be improved upon or eliminated entirely if the iterative procedure were altered to include more variables. In the present work only one of the possible atmospheric parameters in LOWTRAN was allowed to vary in order to obtain synthetic spectra for comparison with the

field data. This parameter, as discussed in chapter 3, was the water-vapor density of the bottom three layers of the model atmosphere. Although this simple approach was functional, a more realistic—in terms of actually simulating atmospheric conditions—approach might be to add an additional element of complexity, and sensitivity, to the fitting procedure and also treat the temperature and pressure profiles and perhaps the CO_2 content of the model atmosphere as variables. To develop this method would require much more experimentation with the LOWTRAN model in combination with a wide variety of remotely-sensed data.

It might also be desireable to develop a continuum-definition scheme which is even more sensitive to the spectral properties of the object surface; if the continuum removal process were expanded and included in the iterative fitting procedure, it could provide the key to improving the fit of the calculated transmission spectra around the regions of the saturated water-vapor bands. The continuum removal process is an important and unique aspect of this calibration scheme; further exploration of its role in the calibration is essential.

Basically only one parameter, the average depths of the water-vapor bands at 0.94μm and 1.13μm, was used to determine the goodness-of-fit between the calculated transmission spectra and the object spectra. A more elaborate calibration scheme could be developed which would use more sophisticated criteria or set of criteria. Some possibilites which might be considered are parameters relating to the changing shape of the water-vapor bands, especially the band near 1.9μm which is nearly coincident with two CO_2 absorption bands. It is quite likely that there is some as yet undiscovered combination of parameters which would be an improvement over the present criteria; these parameters might well be

- 91 -

explored in conjunction with the process discussed above to incorporate other elements of the model atmosphere into the iterative fitting procedure.

3. Inclusion of External Measurements or Field Reflectance Standards

Although the calibration technique developed in this research was conceived as a way of avoiding extensive measurements of a reflectance standard in the field, in fact such measurements, on a much more limited scale, would be useful—if only as a check on the consistency of the system response over time. Additionally, a standard available in the field would provide a means for obtaining data in units of absolute reflectance. Such field-standard measurements could also be important for a satellite-based instrument for which post-flight system recalibration was impractical. In this case, while a ground standard would be ideal, in that it would also provide base atmospheric information, a well-calibrated standard on-board the satellite would at least serve the purpose of establishing the response of the detector system while in operation.

An additional possibility for improving upon the present calibration scheme by incorporating an external measurement into the procedure would be to obtain more traditional atmospheric sounding measurements further into the infrared concurrently with obtaining the near-infrared spectral data. These atmospheric data would then be used much as the near-infrared data are used in the present calibration procedure, but would provide an additional region to "tie-down" the appropriate atmospheric transmission spectra.

The single most important step to take towards improving this calibration scheme, however, is to apply the technique to a greater number and variety of data, measured under diverse conditions. All of the

spectra analyzed in this research were obtained in one geographical locale within a relatively short time-span using one instrument; while the results are very promising, the technique needs to be tested on a broader data set.

B. EXTENSION OF THE TECHNIQUE TO TWO-DIMENSIONAL DATA SETS

An obvious application for the basic calibration procedure developed in this research is to the calibration of two-dimensional (image) data, especially those of high resolution multispectral data produced by such instruments as the Airborne Imaging Spectrometer developed by the Jet Propulsion Laboratory. There are two principal aspects of this application to consider: First, what wavelength sensitivity (i.e. band position and width) would be required in order to employ this model usefully; and, second, practical considerations such as how many of the pixels in an image must actually be calibrated to produce a calibrated image?

1. Spectral Sensitivity Required

A general answer to this question may be obtained from the results of this research. As discussed in chapter 3, the parameter which was found to be most useful in determining the goodness-of-fit of the synthetic atmospheric transmission spectra to the object spectra was the average value of the three points at the minima of the two water-vapor bands centered near $0.94\mu m$ and $1.13\mu m$. These three points encompass a wavelength range of about $0.025\mu m$ for each band (which could possibly be extended to $0.05\mu m$ in each band if, for instance, five points were used). Thus, a wavelength bandwidth comparable to these values, centered on one of these bands, might be used in the application of this spectral calibration procedure to the calibration of images.

2. Practical Considerations

A very simplistic approach to extend the technique developed here to the calibration of two-dimensional data would be to apply this procedure to calibrate each individual pixel of an image; an approach which is seen immediately to be computationally unrealistic. The alternative extreme—applying the technique to calibrate only one pixel in an image and using that atmospheric transmission spectrum to represent the atmospheric components across the entire image—is also unreasonable. In general it is not a valid asumption that the atmosphere is constant across an image; there is not only variation in the atmosphere across the groundtrack represented in a multispectral image, but there is also variation in the solar illumination angle across an image which affects the atmospheric calibration and so must be accounted for (A. Kahle, pers. comm., 1982).

It is not clear at this stage what the extent of the atmospheric variation across a two-dimensional data set might be; it is clear, however, that some compromise between the above two extremes is required if a version of the present technique is to be practically applied. The details of the application must be left to future research, but, in very general terms, there are two approaches which appear promising: The first would require developing an interpolation scheme under which the calibration is actually only performed for some select grid or array of pixels and then extending this set of calibrations across the entire image. Determining the exact grid pattern(s) and interpolation procedure(s) which are most useful and efficient will undoubtedly require extensive work with such a data set. This approach presupposes that the atmospheric variations across the images are not entirely random and that it, in fact, makes sense to interpolate between pixels.

The second approach would utilize some form of reflectance standard on the ground; this would not solve the problem of atmospheric inhomogeneity across the image, but would instead be used to provide the basis for establishing absolute calibration, as well as instrument response over time. The difficulties of using such a standard are discussed in detail in chapter 1; however, the use of a standard in this application would be on a much more limited scale than would be required to calibrate an entire image or groundtrack using only reflectance standards available in the scene.

3. Reduction of Computational Load

Before this calibration procedure may be extended to apply to two-dimensional data, some reduction in the computational load is required. Because the procedure has, thus far, only been applied to a limited number of samples, certain inefficiencies still exist. The most significant of these, in terms of computational time, is that for each iteration in the iterative fitting procedure, a new atmospheric transmission spectrum is calculated. A more practical approach would be to maintain a family of transmission spectra covering a reasonable range of atmospheric conditions and iterate on these parameters without actually recalculating the transmission spectra each time. If necessary, the best-fit transmission spectrum could be obtained from this family of spectra and then the fit could be "fine-tuned" based upon this spectrum.

The second alteration to the procedure is primarily dependent upon the kind of computer available on which to run LOWTRAN. The LOWTRAN code is very generalized; it can be used to perform both transmittance and radiance calculations for several model atmospheres under several configurations, which requires that large files of data and code be maintained. If, as was the case for this research, the amount of

available core memory is limited, then these data must be kept in disk files, rather than in data statements as part of the program code; this substantially increases the amount of time required to perform the calculations. LOWTRAN requires only a few seconds of CPU time on a CDC 6600, it requires about 8 minutes on a Harris 800, about 10 minutes on a Perkin-Elmer 1100, about 35 minutes on a VAX 750 (if the data are kept in disk files) and is too large to be run on an LSI 11/23 without modification. For a given application, it would be beneficial to reduce LOWTRAN to include only the required code and data. This would allow the data to be maintained in core storage during program operation on most machines, including all of the machines mentioned above except possibly the LSI 11/23, and would also substantially decrease the time required to complete the calculations (probably by a factor of at least ten).